J. Fluid Mech. (2026), *vol.* 1032, A65, doi:10.1017/jfm.2026.11421

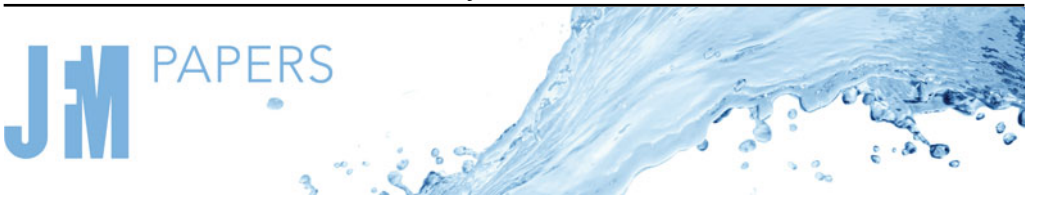

Bottom pressures in a shallow compressible ocean due to nonlinear wave–non-uniform elastic-seafloor interactions

Umesh A. Korde[1] and **S. Elgar**[2]

[1]Environmental and Health Engineering, Johns Hopkins University, Baltimore, MD 21218, USA

[2]Applied Ocean Physics and Engineering, Woods Hole Oceanographic Institution, Woods Hole, MA 02543, USA

Corresponding author: Umesh A. Korde, ukorde1@jhu.edu

(Received 26 February 2025; revised 10 December 2025; accepted 5 March 2026)

The generation and propagation of acoustic-gravity–Scholte wave fields produced by different types of nonlinear interactions between ocean surface waves and shallow, non-uniform depth contours of an elastic seafloor are investigated. Specifically, nonlinear interactions between surface waves and the seafloor, surface waves themselves and the seafloor, and acoustic-gravity-waves and the seafloor are shown to produce resonantly strong bottom pressures. Whereas the interaction between shoreward-propagating surface waves and seafloor depth contours (and the resulting seafloor waves and microseisms) has been discussed in the literature, not much is known about the compression wave–seafloor wave groups forming an important component of the overall energy transfer process in shallow water. Forcing due to the different wave interactions involving the seafloor depth contours and the dispersion relations for the coupled ocean–seafloor system are derived, providing estimates of the energy transfer that results at resonance when the interaction produces a wavenumber–frequency combination that lies on one of the dispersion surfaces for the two-media system. Wavenumber spectra and their temporal evolution are found analytically for stationary random surface-wave fields, and the acoustic-gravity wave potentials, seafloor pressure amplitudes, seafloor power densities and Scholte wave amplitudes are computed, and their sensitivity to critical parameters is estimated. The nonlinear interactions derived here may account for some of the 200 % increase of low-frequency ($0.01 \leqslant f \leqslant 0.03$ Hz) spectral densities of bottom pressure observed between 25 and 8 m water depths in the Atlantic Ocean at a site off Duck,

NC. Further, subject to experimental validation, the power densities estimated here could contribute energy for sensing operations.

Key words: surface gravity waves, elastic waves, shallow water flows

1. Introduction

Wave–wave interactions in deep water have been of great interest for many years (Longuet-Higgins 1950; Phillips 1960; Hasselmann 1962; Hasselmann 1963; Hasselmann 1966, and many others). Such interactions have been studied, for example, as a mechanism for spatial and temporal evolution of surface-wave spectra (Komen & Hasselmann 1996), and as a mechanism for generation (by multidirectional surface-wave interactions) of seafloor microseisms observed during and following the passage of storm systems (Longuet-Higgins 1950; Hasselmann 1963). The contribution of wave–wave interactions in multidirectional surface-wave fields to low-frequency ambient ocean noise in the deep ocean has been quantified (Hughes 1976; Webb & Cox 1986; Kibblewhite 1989). The compression-pressure waves in the water column and surface waves on the seafloor resulting from ocean–surface-wave interactions also have been studied (Ardhuin & Herbers 2013). Numerical solutions to investigate the effect of acoustic-speed variations over the water column on the wave system in the water column and the seafloor have been obtained (Jensen *et al.* 2011). An analytical technique also has been used to study these wave fields in response to seafloor movements (Eyov *et al.* 2013), and studies have investigated the propagation of surface-wave fields generated as part of the seafloor-wave–compression-wave system by seafloor movements (Stiassnie 2010; Abdolali & Kirby 2017; Abdolali, Kadri & Kirby 2019; Meza-Valle, Kadri & Ortega 2023; Williams & Kadri 2023).

A combined wave field comprised of compression waves and seismic waves and its effect on the generation of a surface wave was investigated previously (Abdolali & Kirby 2017; Abdolali *et al.* 2019). The wave field inside the water layer was derived by modelling the compression waves as density variations over the 'reference state' of the ocean where no waves exist (Bondi 1947). The free-surface boundary condition with this formulation includes a gravity term leading to a free-surface velocity. When combined with similar incorporation of the gravity term in the seafloor waves (Abdolali *et al.* 2019), the overall formulation can be used to study the cogeneration of the compression waves, seismic waves and surface waves (e.g. tsunamis) in response to seafloor perturbations. The cogeneration (along with surface waves) by wind gusts of a related wave field termed 'hydroacoustic waves' (Renzi & Dias 2014) was analysed as a solution to an initial-value problem. Also investigated analytically for mildly non-uniform media was the propagation in deep water of wave groups comprised of compression waves in the water and surface waves on the seafloor (Korde 2024), and generated by second-order interactions between multidirectional stationary random surface waves (Hasselmann 1963). That work does not include the gravity term, and considers only the generation of compression waves in water and seafloor waves in response to the forcing of the undisturbed sea surface by a stationary random disturbance provided by the second-order pressure generated by the wave–wave interactions of multidirectional surface waves. Further discussion of the omission of the gravity term for the frequency range of interest here is included in Appendix A.1.

The compression waves in the water are generated by surface-wave interactions, and are referred to as 'acoustic-gravity waves' (Ardhuin & Herbers 2013). Further, the surface waves on the seafloor essentially are Rayleigh waves with the top medium being water rather than air, and hence are termed 'Scholte waves' here.

Acoustic-gravity waves were studied as part of a three-wave resonant triad (Kadri & Akylas 2016) where the amplitude and energy of these waves was estimated under different degrees of tuning. The effect of non-uniform water depth on these waves in deep water was investigated using depth-averaged equations (Renzi 2017). A linear approach was used to derive the dispersion relations for a mildly sloping seafloor (Eyov *et al.* 2013). The effects of other non-uniformities also have been investigated, e.g. the effect of non-uniform water density was studied analytically using a perturbation approach (Michele & Renzi 2020). The effect of mild non-uniformities in propagation velocities in water and the seafloor was studied within a linear formulation to solve for wavenumber–frequency spectra (Korde 2024).

Here, previous work in deep water (Korde 2024) is extended to study acoustic-gravity–Scholte-wave wave groups in shallow water, for which different (and some new) nonlinear interactions potentially have a much larger effect than in deep water. The present treatment provides an analytical approach to determine the statistics of the compression-seafloor wave groups in the form of wavenumber–frequency spectra, and enables comparison with seafloor pressure spectral density results. However, because the gravity term is neglected, it does not quantify the effect of the nonlinear interactions of interest on the surface-wave field. Previous studies of surface-wave interactions in shallow water include: (i) wave–wave interactions in multidirectional wind-wave fields (Freilich & Guza 1984; Elgar & Guza 1985; Herbers & Guza 1991; Kaihatu & Kirby 1992; Kirby 1992; Herbers & Guza 1994; Kaihatu & Kirby 1995, and many others); (ii) interactions between wind-waves or swells and their reflections from shore (Dunnebier *et al.* 2012; Bromirski, Stephen & Gerstoff 2013, and many others); (iii) interactions between swells approaching the shore and the seafloor depth contours (as on a continental shelf, figure 1) (Hasselmann 1963), which have received relatively less attention.

The wave–seafloor interactions were considered as a potential mechanism for generation of low-frequency primary microseisms, such as the observed 27 s period microseisms (Oliver 1962; Hasselmann 1963). It has been proposed that the nonlinear interaction between long swells and a sloping seafloor was one of the mechanisms for the generation of the Earth's hum, particularly in the frequency range $f < 0.1$ Hz (Webb & Crawford 1999; Ardhuin, Gualtieri & Strutzmann 2015). Results for vertical and horizontal components of seafloor pressures due to the interaction of low-frequency, infragravity surface waves with sinusoidal, sloping and randomly varying seafloor geometries were obtained to estimate low-frequency microseism amplitudes (Ardhuin 2018). As discussed above, the complete system has been analysed using three wave equations to model the coupled acoustic–surface-wave system, and the dilatational and distortional waves in the seafloor (Abdolali & Kirby 2017;Abdolali *et al.* 2019). Here, the focus is on nonlinear interactions between surface waves and the seafloor and the compression waves and seafloor waves arising from these interactions. In contrast, most work to date on surface-wave–seafloor interactions considers just their role in the generation of seafloor waves and microseisms. However, these interactions also produce compression waves in the water, and fully accounting for the coupled dynamics of the combined water–seafloor system in shallow water could enable a better understanding of low-frequency seafloor vibrations generated by surface-wave–seafloor interactions. Moreover, such a study is necessary for deriving accurate estimates of the acoustic-gravity-wave power densities at the seafloor for sensing applications in which a long-term source of energy is required. The focus here is on nonlinear wave interactions in shallow water (in which the seafloor plays a prominent role) that lead to resonant excitation of acoustic-gravity and Scholte waves.

Here, the acoustic-gravity–Scholte-waves generated by nonlinear interactions between surface waves and the seafloor (and propagating as groups) are investigated.

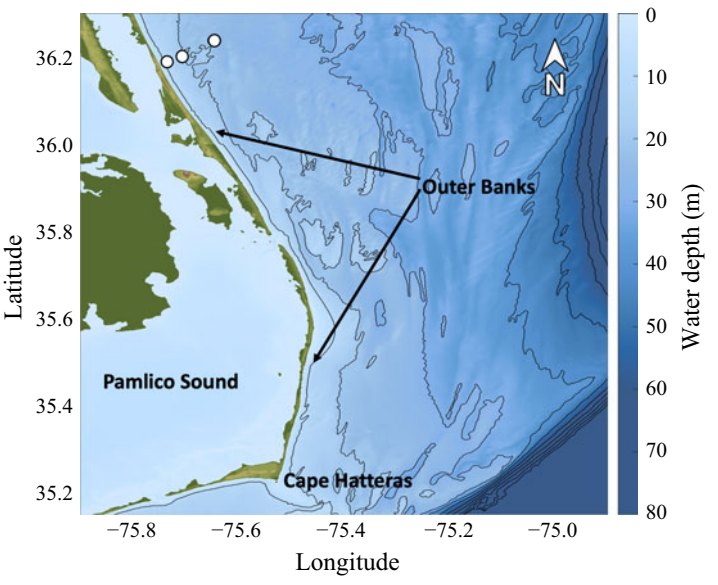

Figure 1. Colour contours of bathymetry (scale on the right-hand y-axis) offshore of the Outer Banks of North Carolina extending from approximately 80 m water depth to the shoreline. Bottom pressures (symbols) were observed in 25, 13 and 8 m water depth. Nonlinear interaction between shoreward-propagating swells and depth contours generates acoustic-gravity–Scholte wave fields in the water-column–seafloor system.

A two-media system comprised of a shallow-water compressible ocean and a sloping elastic seafloor is considered (see § 5 for more details). Given the focus on compression waves in water and just the surface waves on the seafloor, only the top layer of the seafloor is assumed to play an active role. The dissipation constants for propagation of the acoustic-gravity waves over the seafloor (Kibblewhite 1989) were obtained from previous field observations, while for propagation through water (figure 5 in Gottwald 1970) these are derived empirically from published data. The surface-wave elevations, acoustic-gravity waves and Scholte waves are assumed to be stationary random processes. In addition to surface-wave–seafloor interactions, interactions between two surface waves and the seafloor, and acoustic-gravity waves and the seafloor also are considered. The focus is on interactions that excite resonances. The temporal evolution of the wavenumber–frequency spectra for forced waves at the seafloor is derived, and based on these spectra, the Fourier coefficients for seafloor pressures under acoustic-gravity waves, Scholte-wave amplitudes, and the seafloor acoustic-gravity-wave power densities are estimated for forced waves at resonance in the presence of dissipation. Although the setting for the calculations is provided by a seafloor pressure measurement programme near the Outer Banks of North Carolina (figure 1) (Herbers & Guza 1991; Elgar, Herbers & Guza 1994; Herbers & Guza 1994), and the results are compared with the corresponding measurements (Elgar *et al.* 1995), the methods developed here are applicable to most shallow water locations with sloping seafloors. Further, although the calculations are specific to the case when surface waves are normally incident to the seafloor contours, the formulation is applicable for a wider range of conditions. Potential applications include interpretation of seafloor and shore-based microseism records during storms, study of temporal and spatial variability in the Earth's hum, and energy generation at the seafloor from second-order wave–seafloor interactions. The sensitivity of the results to the seafloor elastic parameters, dissipation coefficients and local water depth is investigated analytically.

Expressions for the seafloor pressure resulting from a nonlinear interaction between surface waves and a sloping seafloor are derived in § 2, and other sources of second-order forcing on the seafloor arising from wave–wave interactions are examined in § 3. Interaction between two surface waves and the seafloor is analysed in § 4. The dispersion relations for the shallow-water water-column-variable-depth system are derived in § 5, where the effect of depth non-uniformity on the acoustic-gravity–Scholte wave groups is discussed, and the forcing due to interactions between acoustic-gravity waves and seafloor depth non-uniformities is derived. Generation of forced waves in the two-media system in the presence of dissipation effects is discussed in § 6. The conditions and parameters used in the calculations are summarized in § 7, while the main results, which include frequency spectra for seafloor pressures under forced waves, seafloor pressure amplitudes, seafloor power densities, and Scholte wave amplitudes are presented in § 8. Sensitivity of the results to imprecise knowledge of seafloor elastic parameters, dissipation coefficients and the local water depth is investigated in Appendix A. As discussed in § 8, the nonlinear interactions derived here may account for some of the 200 % increase of low-($0.01 \leqslant f \leqslant 0.03$ Hz) and higher-($f \sim 0.22$ Hz) frequency spectral densities of bottom pressure observed between 25 and 8 m water depths in the Atlantic Ocean at a site offshore of Duck, NC (figure 1).

2. Excitation due to surface-wave–seafloor interactions

When a source of excitation in the water or on the seafloor has a wavenumber and frequency that falls on the dispersion surface for the acoustic-gravity–Scholte wave field in the shallow-water–seafloor coupled system (§ 5), natural modes of the acoustic-gravity–Scholte wave field are excited, causing resonance. Here, the wave field is forced by the external source generated by the nonlinear interaction between surface waves and a non-uniform seafloor (Hasselmann 1963). The surface-wave field is assumed to include both shoreward-propagating waves and their reflections. The method developed in Ardhuin (2018) (main document and Supplementary information) may be used to understand the excitation of acoustic-gravity–Scholte wave groups by surface waves propagating over a non-uniform seafloor. Here a somewhat different approach is investigated, as described below. A coordinate system is introduced where the axes (X, z) are located at the undisturbed free surface, and

$$X = x, \quad z = -H + h(x), \tag{2.1}$$

where x and z are the cross-shore and vertical coordinates, and $h(x)$ describes the bottom profile. Thus, if $h(x) = 0$, $z = -H$. It is assumed here that $h(x)$ is a mildly varying function of x in the sense that a uniform-depth approximation may be used in deriving the boundary conditions as long as the correct depth is substituted at each x in the final steps (Whitham 1973). Under linear finite depth theory, for a particular wavenumber–frequency combination (κ, σ), the z-component $Z(z)$ of the assumed solution $X(x)Z(z)$ to the Laplace equation is

$$Z(z) = C_1 \sinh \kappa z + C_2 \cosh \kappa z, \tag{2.2}$$

where C_1 and C_2 are constants, and κ denotes the surface-wave wavenumber. Letting $\Gamma(x, z; t)$ represent the velocity potential for surface waves, for $X(x) \sim \exp[i(\kappa x - \sigma t)]$, the free surface condition becomes

$$\frac{\partial \Gamma}{\partial z} - \frac{\sigma^2}{g}\Gamma = 0, \tag{2.3}$$

where σ is the surface-wave angular frequency, t is time and g is gravitational acceleration. Substitution of $Z(z)$ from (2.2) into the boundary condition at $z = 0$ implies

$$\kappa C_1 - \frac{\sigma^2}{g} C_2 = 0. \tag{2.4}$$

At the boundary $z = -H + h$, to first order, $\partial \Gamma / \partial z = 0$. This condition implies that

$$\kappa C_1 \cosh \kappa(-H + h) + \kappa C_2 \sinh k(-H + h) = 0. \tag{2.5}$$

Equations (2.4) and (2.5) lead to the surface-wave dispersion relation subject to the mildly variable depth approximation,

$$\sigma^2 = g\kappa \tanh \kappa H \, (1 - h/H). \tag{2.6}$$

The surface-wave velocity potential $\Gamma(x, z; t)$ then becomes

$$\Gamma(x, z; t) = C_2 \left[\frac{\sinh \kappa H(1 - h/H)}{\cosh \kappa H(1 - h/H)} \sinh \kappa z + \cosh \kappa z \right] \exp\left(i(\kappa x - \sigma t)\right). \tag{2.7}$$

Following some algebra,

$$\Gamma(x, z; t) = \frac{C_2 \cosh \kappa \, (z + H(1 - h/H))}{\cosh \kappa H(1 - h/H)} \exp\left(i(\kappa x - \sigma t)\right), \tag{2.8}$$

which can be expressed as

$$\Gamma(x, z; t) = C_2 m_d(\kappa z, \kappa h) \exp\left(i(\kappa x - \sigma t)\right), \tag{2.9}$$

where it is noted that h is a function of x. Here

$$m_d(\kappa z, \kappa h(x)) = \frac{\cosh \kappa \, (z + H(1 - h(x)/H))}{\cosh \kappa H(1 - h(x)/H)}. \tag{2.10}$$

With the coefficient C_2 determined as shown below, $m_d(\kappa z, \kappa h(x))$ in (2.9) describes the modulation of the surface-wave field by variable seafloor topography (cf. equations (9) and (12) in Ardhuin 2018). Further, because the present formulation is in terms of wavenumber–frequency spectra, the spatial modulation of amplitudes of individual wave components is mapped into the wavenumber domain.

The application of the linearized dynamic free-surface condition at $z = 0$,

$$g\zeta = \frac{\partial \Gamma}{\partial t} \tag{2.11}$$

leads to, from (2.8), $C_2 = ig\mathrm{d}Z(\kappa, \sigma)/\sigma$. The dynamic pressure at the seafloor $z = -H + h$ can be expressed as

$$p(x, -H + h; t) = \frac{\rho g \zeta(x, t)}{\cosh \kappa H(1 - h/H)}, \tag{2.12}$$

where ρ is the density of seawater. It can be argued that

$$\cosh \kappa H(1 - h/H) = \cosh(\kappa H - \kappa h) = \cosh kH \cosh \kappa h - \sinh \kappa H \sinh \kappa h, \tag{2.13}$$

and for small h, $\cosh \kappa h \approx 1$ and $\sinh \kappa h \approx \kappa h$, so that

$$\cosh \kappa(H - h/H) \approx \cosh \kappa H - \kappa h \sinh \kappa H = \cosh \kappa H \, (1 - \kappa h \tanh \kappa H). \tag{2.14}$$

Hence,

$$\frac{1}{\cosh \kappa H(1 - h/H)} \approx \frac{1}{\cosh \kappa H} (1 - \kappa h \tanh \kappa H)^{-1} \approx \frac{(1 + \kappa h \tanh \kappa H)}{\cosh \kappa H}. \tag{2.15}$$

The pressure at the seafloor then can be approximated as

$$p(x, -H+h; t) = \rho g \left[\frac{\zeta(x,t)}{\cosh \kappa H} + \frac{\kappa \tan \kappa H}{\cosh \kappa H} \zeta(x,t) h(x) \right], \tag{2.16}$$

where it is made explicit that h is a function of x. The second term in the square brackets contains a product of two x-dependent quantities that can be expressed in the wavenumber domain by means of a Fourier–Stieltjes integral as (Phillips 1960)

$$\int_{\boldsymbol{k}} \mathrm{d}Z_h(\boldsymbol{k}, t) = \iint_{\boldsymbol{\kappa}', \boldsymbol{k}_s} \mathrm{d}Z(\boldsymbol{\kappa}', t) \mathrm{d}H(\boldsymbol{k}_s) \exp\left[i \left(\boldsymbol{\kappa}' + \boldsymbol{k}_s \right) \cdot \boldsymbol{x} \right], \tag{2.17}$$

where bold indicates a vector, $\boldsymbol{\kappa}'$ represents the wavenumber vectors for the surface elevation and $\boldsymbol{k}_s$ denotes the wavenumber vectors for the seafloor. The right-hand side of (2.17) represents infinite combinations of $\boldsymbol{\kappa}'$ and $\boldsymbol{k}_s$ arising from the interaction of the surface wave and the seafloor as approximated above. The surface-wave dispersion relation (2.6) implies that the wavenumber is a function of x for a given frequency, and thus a continuous spectrum of wavenumbers is required to satisfy (2.6), with the seafloor contributing its own wavenumbers. Here, the focus is on a subset of $(\boldsymbol{\kappa}', \boldsymbol{k}_s)$ combinations for which for a given frequency σ the vector sum $\boldsymbol{\kappa}' + \boldsymbol{k}_s$ lies on a dispersion surface for acoustic-gravity waves in the water-column–seafloor system (see § 5). A further restriction is introduced here by choosing $\boldsymbol{\kappa}'$ to be $\boldsymbol{\kappa}_0$ where $\boldsymbol{\kappa}_0$ satisfies the surface-wave dispersion relation at a known depth for a mildly varying seafloor, and the wave–seafloor interaction is observed shoreward of this location. Thus, here the pressure $p(x, -H+h; t)$ is approximated as

$$\begin{aligned} p(x, -H+h; t) &\approx \frac{\rho g \zeta(x; t)}{\cosh \kappa_0 H} + p_\Delta(x, t), \ \text{where} \\ p_\Delta(x, t) &= \frac{\kappa_0 \rho g \tanh \kappa_0 H}{\cosh \kappa_0 H} \zeta(x, t) h(x), \quad \sigma^2 = g \kappa_0 \tanh \kappa_0 H. \end{aligned} \tag{2.18}$$

In terms of wavenumber spectra,

$$p_\Delta(x, t) = \int_{\boldsymbol{k}} \mathrm{d}P_\Delta \mathrm{e}^{i \boldsymbol{k} \cdot \boldsymbol{x}} = \rho g \int_{\boldsymbol{k}_s} \frac{\kappa_0 \rho g \tanh \kappa_0 H}{\cosh \kappa_0 H} \mathrm{d}Z(\boldsymbol{\kappa}_0, t) \mathrm{d}H(\boldsymbol{k}_s) \exp\left[i \left(\boldsymbol{\kappa}_0 + \boldsymbol{k}_s \right) \cdot \boldsymbol{x} \right]. \tag{2.19}$$

Although a more general seafloor profile $h(x)$ such as expanded above and as described in (5.18) and (5.19) (§ 5) could be used, here a depth profile is employed where random features are superimposed on a mildly sloping seafloor, which can be represented as

$$h(x) = bx + cx^2 + \ldots + r(x), \tag{2.20}$$

where $r(x)$ is an amplitude-limited random function of x and may be treated separately (§ 5), and hence is not considered further here. Assuming $c \ll b$, the seafloor profile is simply $h(x) \approx bx$. The slope $b > 0$ for $-\infty < x \leqslant 0$, and $b < 0$ for the image space $0 < x < \infty$. This function is Laplace transformable, and its Fourier transform $F_s(\gamma)$ can be composed using

$$F_s(\gamma) = \int_{-\infty}^{0} b(-x') \mathrm{e}^{-\gamma x'} \mathrm{d}x' + \int_{0}^{\infty} b x' \mathrm{e}^{-\gamma x'} \mathrm{d}x', \tag{2.21}$$

where x' is a dummy variable for the horizontal coordinate, $\gamma = \epsilon + ik_s$ with $0 < \epsilon \ll 1$, and k_s is the seafloor wavenumber. It is seen that, as $\epsilon \to 0$,

$$F_s(\gamma) = F_s(k_s) = \frac{2b}{k_s^2}. \tag{2.22}$$

To force $F_s(k_s)$ to have finite values as $k_s \to 0$ it is written as (Hasselmann 1976)

$$F_s(k_s) = \frac{2b(1-\cos k_s x)}{k_s^2}. \tag{2.23}$$

With two applications of L'Hôspital's rule, the limit of $F_s(k_s)$ as $k_s \to 0$ is

$$\lim_{k_s \to 0} \frac{2(1-\cos k_s x)}{k_s^2} = bx^2. \tag{2.24}$$

As $x \to \infty$ with $k_s \to 0$, the limiting value bx^2 gets increasingly larger, forming a peak with a width decreasing as $1/x$. The Fourier transform $F_s(k_s)$ can then be expressed as $bx\delta(k_s)$, where $\delta(\cdot)$ is the Dirac delta function (Hasselmann 1976). Here, $F_s(k_s)$ is averaged (indicated with an overbar) over the shelf length L_s assuming that $L_w \ll L_s$ where L_w is the surface-wave length. Thus, for $k_s \to 0$,

$$\overline{F_s(k_s)} = \frac{2}{L_s} \int_0^{L_s} bx\delta(k_s)\mathrm{d}x = bL_s\delta(k_s), \quad k_s \to 0. \tag{2.25}$$

Whereas for $k_s > 0$,

$$\overline{F_s(k_s)} = \frac{2}{L_s} \int_0^{L_s} \frac{2(1-\cos k_s x)}{k_s^2}\mathrm{d}x, = \frac{2b}{k_s^2}\left(1 - \frac{\sin k_s L_s}{k_s L_s}\right), \quad k_s > 0. \tag{2.26}$$

Hence,

$$\overline{F_s(k_s)} = \left[bL_s\delta(k_s) + \frac{2b}{k_s^2}\left(1 - \frac{\sin k_s L_s}{k_s L_s}\right)\right]. \tag{2.27}$$

The seafloor profile now can be represented as

$$h(x) = \frac{1}{2\pi} \int_{k_s} \overline{\mathrm{d}F_s(k_s)} \exp(i\boldsymbol{k}_s \cdot \boldsymbol{x}), \ \overline{\mathrm{d}F_s(k_s)} = \overline{F_s(k_s)}\mathrm{d}k_s, \tag{2.28}$$

where k_s is the magnitude of $\boldsymbol{k}_s$. Here $\overline{\mathrm{d}F_s(k)}$ is the Fourier–Stieltjes representation $\mathrm{d}H$ in (2.19). Here

$$\mathrm{d}P_\Delta(\boldsymbol{k}, t) = \rho g \left[\left(\kappa_0 \frac{\mathrm{d}Z(\boldsymbol{\kappa}_0, t)\tanh \kappa_0 H}{\cosh \kappa_0 H}\right)\overline{\mathrm{d}F_s(\boldsymbol{k}_s)}\right], \ \boldsymbol{k} = \boldsymbol{\kappa} + \boldsymbol{k}_s. \tag{2.29}$$

The surface-wave wavenumber ($\boldsymbol{\kappa}$) in the following is the same as that in (2.18), with the subscript 0 dropped. The seafloor pressure Fourier coefficient as shown in (2.29) indicates that the resulting pressure results from an interaction between the surface wave and the seafloor and depends on the surface wavenumber $\boldsymbol{\kappa}$ and the seafloor wavenumber $\boldsymbol{k}_s$ and has a wavenumber $\boldsymbol{k}$ as determined by the vector sum of $\boldsymbol{\kappa}$ and $\boldsymbol{k}_s$. This pressure leads to an acoustic-gravity–Scholte wave group at a wavenumber–frequency combination $(\boldsymbol{k}, \omega)$, where $\omega = \sigma$. For propagation along the x-axis, the temporal evolution of the wavenumber

spectrum $S_{P_\Delta}(\boldsymbol{k}, t)$ for $\mathrm{d}P_\Delta(\boldsymbol{k}, t)$ can be found as

$$\mathrm{d}P_\Delta \mathrm{d}P_\Delta = \rho^2 g^2 \left(\frac{\kappa \tanh \kappa H}{\cosh \kappa H}\right)^2 \mathrm{d}Z(\kappa, t)\mathrm{d}Z^*(\kappa, t)\overline{\mathrm{d}F_s(k_s)\mathrm{d}F_s^*(k_s)}. \tag{2.30}$$

When $\boldsymbol{\kappa}$ is determined as described above (cf. (2.18),

$$S_{P_\Delta}(\boldsymbol{k}, t) = \frac{\mathrm{d}P_\Delta \mathrm{d}P_\Delta^*}{\mathrm{d}\boldsymbol{k}}, \tag{2.31}$$

which can be expressed as

$$S_{P_\Delta}(\boldsymbol{k}, t) = \rho^2 g^2 \iint\limits_{\boldsymbol{\kappa}\boldsymbol{k}_s} \left(\frac{\tanh \kappa H}{\cosh \kappa H}\right)^2 \kappa^2 S_e(\boldsymbol{\kappa}, t) S_{sf}(\boldsymbol{k}_s)\delta(\boldsymbol{k} - \boldsymbol{\kappa} - \boldsymbol{k}_s)\mathrm{d}\boldsymbol{\kappa}\mathrm{d}\boldsymbol{k}_s, \tag{2.32}$$

where S_e is the wavenumber spectrum of the surface waves and S_{sf} is the wavenumber spectrum of the seafloor. Here $S_{P_\Delta}(\boldsymbol{k}, t)$ provides the forcing for the acoustic-gravity wave field generated by the interaction of the surface waves with the sloping bottom. Equation (2.32) can be expressed in terms of wavenumber–frequency spectra via a Fourier–Stieltjes expansion into wavenumber space. Resonance occurs for propagation in the x direction when for a particular frequency ω, the wavenumber k is such that (k, ω) lie on a dispersion surface for an acoustic-gravity–Scholte wave group excited by the pressure-spectrum in equation (2.32). The present approach for modelling the seafloor slope is convenient and is general enough to allow extensions to more complicated seafloor topographies.

3. Direct second-order pressure generation

Except as the water depth approaches zero, three surface waves with frequencies σ_1, σ_2 and σ_3 where $\sigma_1 + \sigma_2 = \sigma_3$ do not have corresponding wavenumbers that satisfy the resonance condition $\boldsymbol{\kappa}_1 + \boldsymbol{\kappa}_2 = \boldsymbol{\kappa}_3$ (Phillips 1960; Hasselmann 1962). However, a three-wave interaction such as

$$\begin{aligned} \boldsymbol{\kappa}_1 + \boldsymbol{\kappa}_2 &= \boldsymbol{k}, \\ \sigma_1 + \sigma_2 &= \omega \end{aligned} \tag{3.1}$$

can produce a combination $(\boldsymbol{k}, \omega)$ that lies on one (or more) of the dispersion surfaces for an acoustic-gravity–Scholte wave field and hence can excite an energetic acoustic-gravity wave field.

The nonlinear terms $\nabla_h \Gamma \cdot \nabla_h \zeta$, $(\partial\Gamma/\partial z)^2$ and $\zeta(\partial^2\Gamma/\partial z^2)$ also contribute to the second-order pressures on the seafloor (∇_h denotes the gradient operator with just the horizontal components included, to distinguish it from the gradient operator ∇ as used elsewhere) (Ardhuin & Herbers 2013). The three terms are considered further in the following.

Using the surface elevation ζ based on linear theory, the Fourier–Stieltjes expansion for the pressure term $p_{d1}(\boldsymbol{x}, t)$ corresponding to $\nabla_h \Gamma \cdot \nabla_h \zeta$ at $\zeta = 0$ can be expressed as

$$\begin{aligned} p_{d1}(\boldsymbol{x}, t) = -\rho g^2 \iint\limits_{\boldsymbol{\kappa},\boldsymbol{\kappa}'} \iint\limits_{\sigma,\sigma'} \frac{\boldsymbol{\kappa} \cdot \boldsymbol{\kappa}'}{\sigma\sigma'} \frac{\cosh \kappa(z + H - h)}{\cosh \kappa(H - h)} \\ \times \mathrm{d}Z(\boldsymbol{\kappa}, \sigma)\mathrm{d}Z'(\boldsymbol{\kappa}', \sigma') \exp\left[\left(\boldsymbol{\kappa} + \boldsymbol{\kappa}'\right) \cdot \boldsymbol{x} - \left(\sigma + \sigma'\right) t\right]. \end{aligned} \tag{3.2}$$

Similarly, the pressure terms $p_{d2}(\boldsymbol{x}, t)$ and $p_{d3}(\boldsymbol{x}, t)$ corresponding to $(\partial\Gamma/\partial z)^2$, and $\zeta(\partial^2\Gamma/\partial z^2)$ can be expressed in terms of their Fourier–Stieltjes expansions as

$$p_{d2}(\boldsymbol{x},t) = -\rho g^2 \iint\limits_{\boldsymbol{\kappa}\boldsymbol{\kappa}'} \iint\limits_{\sigma\sigma'} \frac{\kappa\kappa'}{\sigma\sigma'} \left(\frac{\sinh\kappa(z+H-h)}{\cosh\kappa(H-h)}\right)\left(\frac{\sinh\kappa'(z+H-h)}{\cosh\kappa'(H-h)}\right) \times \exp\left[\left(\boldsymbol{\kappa}+\boldsymbol{\kappa}'\right)\cdot\boldsymbol{x} - \left(\sigma+\sigma'\right)t\right], \tag{3.3}$$

and

$$p_{d3}(\boldsymbol{x},t) = -\rho g^2 \iint\limits_{\boldsymbol{\kappa}\boldsymbol{\kappa}'} \iint\limits_{\sigma\sigma'} \frac{\boldsymbol{\kappa}\cdot\boldsymbol{\kappa}'}{\sigma\sigma'} \mathrm{d}Z(\boldsymbol{\kappa},\sigma)\mathrm{d}Z'(\boldsymbol{\kappa}',\sigma') \exp\left[\left(\boldsymbol{\kappa}+\boldsymbol{\kappa}'\right)\cdot\boldsymbol{x} - \left(\sigma+\sigma'\right)t\right]. \tag{3.4}$$

For all three pressure components, for the unidirectional case when κ and κ' are both shoreward propagating,

$$\begin{aligned} \kappa + \kappa' &= k, \\ \sigma + \sigma' &= \omega. \end{aligned} \tag{3.5}$$

Here $k > \kappa, \kappa'$ and $\omega > \sigma, \sigma'$ for the wavenumbers and frequencies commonly observed in surface gravity wave spectra in the (0.01, 2.00) Hz range. No wavenumbers κ for such waves are small enough to form a combination (κ, σ) that lies on one of the first three acoustic-gravity dispersion surfaces (wave scattering can be significant for higher modes (Hasselmann 1963; Jensen *et al.* 2011)), and thus the second-order terms do not lead to resonant interactions and hence do not produce longer-lasting interactions such as the surface-wave–seafloor interactions examined in § 2. An interaction between oppositely propagating incident (I) and reflected (R) surface waves would produce an acoustic-gravity wave field with $\boldsymbol{k} = 0$, and $\omega = 2\sigma$. The dispersion relation defining this wave field is given by (Jensen *et al.* 2011; Korde 2024)

$$\alpha \tan\alpha H = \frac{\lambda' + 2\mu'}{\lambda}\alpha', \quad \alpha = \frac{\omega}{c_1}, \quad \alpha' = \frac{\omega}{c_p}, \tag{3.6}$$

where λ and λ' are Lamé constants associated with dilatation of the fluid particles and of the seafloor, respectively, μ' is the Lamé constant associated with distortion of the seafloor, c_1 denotes the acoustic velocity in salt water and c_p is the dilatational wave velocity in the seafloor.

In the limiting case of a rigid seafloor, $\lambda', \mu' \to \infty$, and

$$\begin{aligned} &\tan\alpha H \to \infty, \ \Rightarrow \cos\alpha H \to 0, \\ &\text{or,} \ \frac{\omega_n H}{c_1} \to (2n+1)\frac{\pi}{2}, \ n = 0,\ 1,\ 2,\ \ldots, \end{aligned} \tag{3.7}$$

because $k = 0$ (Longuet-Higgins 1950; Kadri & Akylas 2016; Korde 2024). The resonance frequencies for the elastic seafloors would be in the neighbourhood of these ω_n values. The fundamental-mode ($n = 0$) resonance frequency for $H \to 13$ m is approximately 28 Hz, which is far out of the frequency range of surface-gravity wave spectra.

For the shallow water depths ($\sim O(10\,\mathrm{m})$) resonance can be expected only for the higher modes $n \geqslant 3$, for which scattering effects may be large and the resulting acoustic-gravity wave field may not be sufficiently energetic.

For these reasons, the second-order pressure generation mechanisms described above are not considered further, and the focus is on wave interactions in which the seafloor plays a role. Interactions between incident and reflected waves of nearly equal frequencies and the seafloor are considered in § 4.

4. Wave–wave–seafloor interactions

Two types of three-wave interaction in shallow water are considered here: (i) one involving a shoreward-propagating wave, a reflected wave and the seafloor; (ii) the other involving the difference frequency wave resulting from quadratic interaction of two shoreward waves and the seafloor. Wave–wave–seafloor interactions generating another surface wave have been investigated (Arduin, Drake & Herbers 2002). In contrast, the object here is to study such interactions when they lead to acoustic-gravity waves. An interaction between incident and reflected waves of unequal, but comparable frequencies and a sloping seafloor can lead to a resonant combination $(\boldsymbol{k}, \omega)$ such that

$$\begin{aligned} \boldsymbol{\kappa}_I + \boldsymbol{\kappa}_R + \boldsymbol{k}_s &= \boldsymbol{k}, \\ \sigma_I + \sigma_R + 0 &= \omega. \end{aligned} \tag{4.1}$$

For unidirectional surface waves and seafloor contours,

$$\begin{aligned} \kappa_I - \kappa_R - k_s &= k, \\ \sigma_I + \sigma_R &= \omega, \end{aligned} \tag{4.2}$$

where (k, ω) is a point on the acoustic-gravity–Scholte wave dispersion curve for the depth H and the known λ, λ' and μ'.

Other interactions of interest here involve difference-frequency waves resulting from quadratic interactions between two shoreward propagating waves with closely spaced frequencies. Nonlinear interaction of these low-frequency, low-wavenumber waves with the seafloor could produce energetic acoustic-gravity and Scholte waves. When the wave components are normal to the seafloor contours,

$$\begin{aligned} \kappa_1 - \kappa_2 - k_s &= k, \\ \sigma_1 - \sigma_2 &= \omega. \end{aligned} \tag{4.3}$$

Letting κ represent κ_I or κ_1 and κ' denote κ_R or κ_2, the treatment below can be applied to both types of interaction ((4.2) and (4.3)). Specifically, the free-surface boundary condition is linearized and satisfied at the undisturbed free surface $z = 0$. It is proposed that the wave–wave–seafloor interactions of interest can be understood as a second-order interaction between two surface waves as represented by the quantity $(\nabla \Gamma)^2$ (where ∇ represents the full gradient) and its second-order interaction with the seafloor. In shallow water over a flat seafloor, the pressure resulting from the $(\nabla \Gamma)^2$ term is cancelled by the pressure from the u^2 term at the seafloor (Ardhuin & Herbers 2013). When the seafloor profile is mildly non-uniform the $\partial \Gamma / \partial z$ term is non-zero at second order, which also results in second-order variation in the horizontal velocity (because $\nabla \cdot \boldsymbol{u} = 0$). The goal here is to quantify the pressure resulting from second-order interactions between the $(\nabla \Gamma)^2$ term and the seafloor profile.

The pressure spectrum due to the $(\nabla \Gamma)^2$ at $z = 0$ is evaluated for two interacting surface waves using a modified form of the spectrum in Hasselmann (1963) that includes a depth correction factor $d_c = \tanh \kappa H \tanh \kappa' H$ attached to the wavenumber product representing the vertical derivatives,

$$\begin{aligned} S'_e(\boldsymbol{k}', \omega) = g^4 \iint\limits_{\boldsymbol{\kappa}, \sigma} \iint\limits_{\boldsymbol{\kappa}', \sigma'} S_\zeta(\boldsymbol{\kappa}, \sigma) S_{\zeta'}(\boldsymbol{\kappa}', \sigma') \frac{\left(\kappa \kappa' d_c - \boldsymbol{\kappa} \boldsymbol{\kappa}'\right)^2}{(\sigma \sigma')^2} \delta\left(\boldsymbol{k}' - \boldsymbol{\kappa} - \boldsymbol{\kappa}'\right) \\ \times \delta\left(\omega - \sigma \mp \sigma'\right) \mathrm{d}\boldsymbol{\kappa} \, \mathrm{d}\boldsymbol{\kappa}' \mathrm{d}\sigma \mathrm{d}\sigma'. \end{aligned} \tag{4.4}$$

Equation (4.4) is consistent with (A.2) in (Ardhuin & Herbers 2013) when applied at $z = 0$.

The wavenumber spectrum in (4.4) is based on the second-order pressure as defined by $\rho(\nabla\Gamma)^2$, where the gradient operator includes the vertical component (the terms $\kappa\kappa'$ appearing alongside the terms $\boldsymbol{\kappa}\cdot\kappa'$ in (2.12) in Hasselmann (1963), which was adapted into equation (5.5) in Korde (2024)),

$$\begin{aligned}\boldsymbol{\kappa}+\boldsymbol{\kappa}'&=\boldsymbol{k}',\\ \sigma\pm\sigma'&=\omega.\end{aligned}\tag{4.5}$$

The pressure variation due to $(\nabla\Gamma)^2$ acts at $z=0$. The effect of this pressure variation can be replaced by an equivalent free-surface elevation ζ_{eq} given by

$$\zeta_{eq}=\frac{(\nabla\Gamma)^2}{2g}.\tag{4.6}$$

The interaction of the equivalent surface elevation ζ_{eq} with the seafloor can be evaluated using the method of § 2 for propagation in the x direction, starting with

$$p_{\Delta q}(x,-H+h;t)=\rho g\frac{k'\tan k'H}{\cosh k'H}\zeta_{eq}(x,t)h(x).\tag{4.7}$$

Subsequent steps similar to those in § 2 lead to

$$S_{Ps}(\boldsymbol{k},t)=\rho^2g^2\iint\limits_{\boldsymbol{k}'\boldsymbol{k}_s}\boldsymbol{k}'\cdot\boldsymbol{k}'S'_{eq}(\boldsymbol{k}',t)S_{sf}(\boldsymbol{k}_s)\delta(\boldsymbol{k}-\boldsymbol{k}'-\boldsymbol{k}_s)\mathrm{d}\boldsymbol{k}'\mathrm{d}\boldsymbol{k}_s,\tag{4.8}$$

where, using (4.6),

$$S_{eq}(\boldsymbol{k}',t)=\frac{S'_e(\boldsymbol{k}',t)}{(2g)^2}.\tag{4.9}$$

Equation (4.9) can be expressed in terms of wavenumber–frequency spectra via a Fourier–Stieltjes expansion into wave frequency space. This pressure variation at the seafloor (representing the two types of wave–wave–seafloor interactions above) contributes one source of excitation to the acoustic-gravity–Scholte wave field in the two media system comprised of the water column and the seafloor (see § 5). The temporal evolution of the acoustic-gravity–Scholte wave field can then be derived using the approach summarized in § 6.

5. Acoustic-gravity–Scholte wave field in shallow water over non-uniform depth

Amplitude variations for acoustic-gravity waves in shoaling depths were computed using energy flux arguments (Eyov *et al.* 2013), and a perturbation approach within a depth-averaged formulation (Renzi 2017) was used to evaluate the amplitudes and frequencies of acoustic-gravity waves over a mildly sloping seafloor. Here, an approach based on the coupled mechanics of acoustic-gravity and Scholte waves is employed, and the different wave fields are assumed to be stationary random processes. Wavenumber–frequency spectra are derived for a wave field comprised of compression waves in the shallow ocean layer and Scholte waves on a linearly sloping seafloor with random features superimposed. A perturbation approach is used to accommodate the depth non-uniformity.

The domain consists of a finite ocean layer and a semi-infinite seafloor layer. Surface-wave forcing by the acoustic-gravity–Scholte wave field represented by a gravity term (Bondi 1947; Abdolali & Kirby 2017) is neglected because it is relatively small for the frequency range considered here (see § 6 and Appendix A) given the focus on the nearshore acoustic-gravity–Scholte wave groups. However, inclusion of the gravity term

in the equations of motion impacts the phase velocities of generated wave fields for long wavelengths in the presence of water compressibility and seafloor elasticity (Abdolali *et al.* 2019), and the treatment below is limited to frequencies $f \geqslant 0.01$ Hz. However, inclusion of the gravity term in the derivation of the dispersion relations below would enable an extension of the results here to include similar interactions with longer-period, lower-frequency waves.

Ocean floors generally have properties varying with depth below the seabed, and often a multilayer approximation for the semi-infinite seafloor (each with different elastic constants and densities (Dziewonski & Anderson 1981)) is used. A multilayer model with one layer modelling the ocean and six layers representing the seafloor was investigated in $\sim$100 m water depths (Kibblewhite & Wu 1993). Although a multilayered seafloor representation would be preferred in a study that includes seismic surface waves and body waves (e.g. P and S waves) generated by sea–surface-wave interactions, here the focus is on seafloor surface waves that decay rapidly with depth. Thus, here the seafloor is represented as a single layer with properties averaged over the top ~ 1000 m. The origin is located at the seafloor with the x axis along the propagation direction approaching from $x \to -\infty$, with the y axis pointing vertically up (Korde 2024). The shore is at a distance L_s along the propagation direction. Part of the wave field is assumed to be reflected back from the shore, with the rest manifesting as a Rayleigh wave propagating along the land surface. The effect of shore reflection is modelled using an image domain from L_s to ∞. Assuming L_s to be long, the entire domain is taken to be $-\infty < x < \infty$ and $0 \leqslant y \leqslant H - h$, where H denotes the water depth measured from $y = 0$ at the bottom of the continental shelf, and $y = h(x)$ represents the seafloor profile superimposed over the plane $y = 0$. Part of the goal is to derive the dispersion relation relating $\boldsymbol{k}$, α and ω for the coupled compression-wave–seafloor-wave system, where $\boldsymbol{k}$ denotes the horizontal wavenumber, α denotes the vertical wavenumber and ω is the angular frequency of the wave field. Free acoustic-gravity–Scholte wave groups (such as created by impulsive plate movement or an underwater explosion) satisfy the dispersion relation, and resonance occurs when wavenumber–frequency combinations for acoustic-gravity–Scholte waves forced by interacting surface waves or surface-wave–seafloor interactions satisfy the dispersion relation. The dispersion relation defines multiple compression-wave–seafloor-wave modes, with each mode defining a unique dispersion surface.

The underwater wave field must satisfy the interface conditions at the water–air interface $y = H - h$ and at the water–seafloor interface $y = h$, $h \neq 0$, in addition to the radiation condition that the waves are incoming at $x \to -\infty$ and outgoing at $x \to \infty$. The water layer can support only dilatational waves (here referred to as compression waves or acoustic-gravity waves) for which $\phi(x, t)$ denotes the scalar displacement potential, which defines the displacement vector as

$$\boldsymbol{u} = \nabla\phi, \quad \text{or } u = \frac{\partial\phi}{\partial x}, \quad v = \frac{\partial\phi}{\partial y}. \tag{5.1}$$

The seafloor can support dilatational and distortional (i.e. shear mode) waves, requiring a scalar potential $\phi'(x, t)$ and a vector potential $\boldsymbol{\Psi}$. For propagation in the x direction, only the vertical shear mode exists, so that $\boldsymbol{\Psi} = [0, \ \Psi_y]^T$. The seafloor displacements u' and v' ($'$ denoting seafloor) can be expressed as

$$\boldsymbol{u}' = \nabla\phi' + \nabla \times \boldsymbol{\Psi}. \tag{5.2}$$

Thus,

$$u' = \frac{\partial\phi'}{\partial x} + \frac{\partial\Psi_y}{\partial y}, \text{ and } v' = \frac{\partial\phi'}{\partial y} - \frac{\partial\Psi_y}{\partial x}. \tag{5.3}$$

The boundary condition at $y = h(x)$, or $f(x, y) = y - h(x) = 0$ is that the fluid and solid particles on either side of the seafloor remain in contact with the seafloor and hence their components normal to the seafloor are equal. Thus (Whitham 1973),

$$\frac{\mathrm{d}f}{\mathrm{d}t} = \frac{\partial f}{\partial t} + u\frac{\partial f}{\partial x} + v\frac{\partial f}{\partial y} = 0,$$
$$\frac{\mathrm{d}f}{\mathrm{d}t} = \frac{\partial f}{\partial t} + u'\frac{\partial f}{\partial x} + v'\frac{\partial f}{\partial y} = 0. \tag{5.4}$$

Since the seafloor shape is independent of time at the time scales of this problem, (5.4) leads to

$$v - u\frac{\mathrm{d}h}{\mathrm{d}x} = 0, \text{ and } v' - u'\frac{\mathrm{d}h}{\mathrm{d}x} = 0. \tag{5.5}$$

Subtracting the second equation from the first,

$$(v - v') - (u - u')\frac{\mathrm{d}h}{\mathrm{d}x} = 0. \tag{5.6}$$

The boundary condition at the free-surface $y = H - h$ is kinetic and requires that the normal stress τ_{yy} opposing fluid oscillation at the free surface equal the pressure p on the free surface. That is

$$\tau_{yy} = \lambda\left(\frac{\partial u}{\partial x} + \frac{\partial v}{\partial y}\right) = p, \tag{5.7}$$

where λ is a Lamé constant associated with dilatation of the fluid particles and p denotes the pressure field at the free surface due to wave–wave and wave–seafloor interactions. For free waves, $p = 0$. At the fluid–solid interface at $y = h$, the normal stress on the water side must equal the normal stress on the seafloor side. The stress components normal to and tangential to the inclined seafloor at (x, h) are given by the terms with overbars,

$$\overline{\tau}_{yy} = \frac{\tau_{xx} + \tau_{yy}}{2} - \frac{\tau_{xx} - \tau_{yy}}{2}\cos 2\theta' - \tau_{xy}\sin 2\theta',$$
$$\overline{\tau}_{xy} = \frac{\tau_{yy} - \tau_{xx}}{2} + \tau_{xy}\cos 2\theta'. \tag{5.8}$$

Here, θ' denotes the local angle of inclination of the seafloor such that $\tan\theta'$ is the local slope of the seafloor. Assuming θ' to be small, to first order,

$$\tan\theta' \approx \sin\theta' \approx \theta', \quad \text{and} \quad \cos\theta' \approx 1. \tag{5.9}$$

The horizontal stress component on a flat seafloor on the water side is $\tau_{xx} = 0$, because the horizontal oscillation is not opposed in the absence of viscous friction, which is neglected here. The shear stress is zero because the fluid cannot support shear oscillations. The stress components on the inclined seafloor $y = h(x)$ are (Auld (1990), chapters 1 and 2)

$$\overline{\tau}_{yy} = \tau_{yy}, \text{ and}$$
$$\overline{\tau}_{xy} = \frac{\tau_{yy}}{2}\sin 2\theta \approx \frac{\tau_{yy}}{2}2\theta' \approx \tau_{yy}\frac{\mathrm{d}h}{\mathrm{d}x}. \tag{5.10}$$

On the solid side, the shear stress is non-zero, and

$$\overline{\tau}'_{yy} = \tau'_{yy} - 2\tau'_{xy}\frac{\mathrm{d}h}{\mathrm{d}x},$$
$$\overline{\tau}'_{xy} = \tau'_{xy} + \tau'_{yy}\frac{\mathrm{d}h}{\mathrm{d}x}. \tag{5.11}$$

The kinetic conditions at $y = h$ are

$$\overline{\tau}_{yy} = \overline{\tau}'_{yy}, \text{ and}$$
$$\overline{\tau}_{xy} = \overline{\tau}'_{xy}. \tag{5.12}$$

It is easier to work in the original coordinate system as long as the relationships in (5.11) and (5.12) are correctly applied. The stress components on the solid side of the seafloor are related to the particle displacements in the solid as

$$\tau'_{yy} = \lambda' \left(\frac{\partial u'}{\partial x} + \frac{\partial v'}{\partial y} \right) + 2\mu' \frac{\partial v'}{\partial y}, \text{ and}$$
$$\tau'_{xy} = \mu' \left(\frac{\partial u'}{\partial y} + \frac{\partial v'}{\partial x} \right). \tag{5.13}$$

It follows that, at $y = h$,

$$\lambda \left(\frac{\partial u}{\partial x} + \frac{\partial v}{\partial y} \right) = \lambda' \left(\frac{\partial u'}{\partial x} + \frac{\partial v'}{\partial y} \right) + 2\mu' \frac{\partial v}{\partial y} - 2\mu' \left(\frac{\partial u'}{\partial y} + \frac{\partial v'}{\partial x} \right), \text{ and}$$
$$\lambda \left(\frac{\partial u}{\partial x} + \frac{\partial v}{\partial y} \right) \frac{\mathrm{d}h}{\mathrm{d}x} = \mu' \left(\frac{\partial u'}{\partial y} + \frac{\partial v'}{\partial x} \right) + \left[\lambda' \left(\frac{\partial u'}{\partial x} + \frac{\partial v'}{\partial y} \right) + 2\mu' \frac{\partial v'}{\partial y} \right] \frac{\mathrm{d}h}{\mathrm{d}x}. \tag{5.14}$$

Although the seafloor bathymetry $h(x)$ may be known, it could be represented as an approximately known depth variation function with a random term added. Further, because $\partial h/\partial x$ is dimensionless, (5.6) has the dimension of the deflections u, v, u' and v'. Hence, even though a perturbation series is needed for investigating nonlinear interactions, the expansions may be applied to the original equations without affecting the dimensions of the terms appearing in the expansions for each order. Here, $\epsilon = h_a k_a / 2\pi$ is used as a perturbation parameter, with h_a denoting the nominal depth of the seafloor, and k_a a nominal wavenumber in the acoustic-gravity wave field. For the ith dispersion mode, ${}^i\phi$, ${}^i\phi'$ and ${}^iH_y$ are expanded as

$$\begin{aligned} {}^i\phi &= {}^i\phi_1 + {}^i\phi_2 + {}^i\phi_3 + \ldots, \\ {}^i\phi' &= {}^i\phi'_1 + {}^i\phi'_2 + {}^i\phi'_3 + \ldots, \\ {}^iH_y &= {}^iH_{y1} + {}^iH_{y2} + {}^iH_{y3} + \ldots, \end{aligned} \tag{5.15}$$

with ${}^i\phi_1 = {}^i\phi_1$, each subsequent order in the expansion can be expressed as ${}^i\phi_2 = \epsilon {}^i\phi_1$, ${}^i\phi_3 = \epsilon^2 {}^i\phi_1$, and so forth (Hasselmann 1966). The acoustic-gravity–Scholte wave field resulting from a stationary random surface-wave field also is a stationary random process, and thus the potentials are expanded using Fourier–Stieltjes integrals as

$${}^i\phi_j = \iint^{i} k_j, {}^i\omega_j \left({}^i\mathrm{d}A_{j1} \cos {}^i\alpha_j y + {}^i\mathrm{d}A_{j2} \sin {}^i\alpha_j y \right) \exp\left({}^ik_j x - {}^i\omega_j t \right), \ i, j = 1, 2, 3, \ldots,$$

$${}^i\phi'_j = \iint^{i} k_j, {}^i\omega_j ({}^i\mathrm{d}A'_j \exp\left({}^i\alpha'_j y \right) \exp({}^ik_j x - {}^i\omega_j t), \ i, j = 1, 2, 3, \ldots,$$

$${}^iH_{yj} = \iint^{i} k_j, {}^i\omega_j ({}^i\mathrm{d}B'_j \exp\left({}^i\beta'_j y \right) \exp\left({}^ik_j x - {}^i\omega_j t \right), \ i, j = 1, 2, 3, \ldots. \tag{5.16}$$

Here,

$$
\begin{aligned}
{}^{i}\alpha_j &= \sqrt{\left({}^{i}\omega_j^2/c_1^2 - {}^{i}k_j^2\right)},\\
{}^{i}\alpha'_j &= \sqrt{\left({}^{i}k_j^2 - {}^{i}\omega_j^2/c_p^2\right)},\\
{}^{i}\beta'_j &= \sqrt{\left({}^{i}k_j^2 - {}^{i}\omega_j^2/c_s^2\right)}.
\end{aligned}
\tag{5.17}
$$

A real-valued ${}^{i}\alpha_j$ represents an oscillatory wave solution in the water (for mode i and expansion order j), whereas real-valued ${}^{i}\alpha'_j$ and ${}^{i}\beta'_j$ represent an exponentially decreasing solution for the vertical oscillations within the solid (Korde 2024). The seafloor $y = h(x)$ can be expanded as

$$
h(x) = H_1 + H_2 + H_3 + \ldots. \tag{5.18}
$$

with

$$
H_j = \int_{k_{sj}} \mathrm{d}H_j \exp(-ik_{sj}x), \quad j = 1, 2, 3, \ldots. \tag{5.19}
$$

If the seafloor shape $y = h(x)$ is such that $h(x)$ can be treated as small, then the trigonometric and exponential functions containing h (via y) in the expansions of equation (5.16) can be approximated to third order as

$$
\begin{aligned}
{}^{i}\mathrm{d}A_{1j}\cos{}^{i}\alpha_j h + {}^{i}\mathrm{d}A_{2j}\sin{}^{i}\alpha_j h \approx {}^{i}\mathrm{d}A_{1j}&\left(1 + \frac{\left({}^{i}\alpha_j h\right)^2}{2!} + \ldots\right)\\
&+ {}^{i}\mathrm{d}A_{2j}\left(\left({}^{i}\alpha_j h\right) + \frac{\left({}^{i}\alpha_j h\right)^3}{3!} + \ldots\right),
\end{aligned}
\tag{5.20}
$$

and

$$
\begin{aligned}
{}^{i}\mathrm{d}A'_j \exp\left({}^{i}\alpha'_j h\right) &\approx {}^{i}\mathrm{d}A'_j\left(1 + {}^{i}\alpha'_j h + \frac{\left({}^{i}\alpha'_j h\right)^2}{2!} + \frac{\left({}^{i}\alpha'_j h\right)^3}{3!} + \ldots\right),\\
{}^{i}\mathrm{d}B'_j \exp\left({}^{i}\beta'_j h\right) &\approx {}^{i}\mathrm{d}B'_j\left(1 + {}^{i}\beta'_j h + \frac{\left({}^{i}\beta'_j h\right)^2}{2!} + \frac{\left({}^{i}\beta'_j h\right)^3}{3!} + \ldots\right).
\end{aligned}
\tag{5.21}
$$

The Fourier–Stieltjes expansions in (5.16) with the approximations in (5.20) and (5.21) are substituted into the four boundary conditions for the ocean–seafloor system. Carrying out the analysis up to third order, the following equations result:

order one,

$$
\begin{aligned}
-\lambda({}^{i}k_1^2 + {}^{i}\alpha_1^2)\left({}^{i}\mathrm{d}A_{11}\cos{}^{i}\alpha_1 H + {}^{i}\mathrm{d}A_{21}\sin{}^{i}\alpha_1 H\right) &= 0,\\
{}^{i}\alpha_1^{i}\mathrm{d}A_2 - {}^{i}\alpha'_1{}^{i}\mathrm{d}A'_1 + i^{i}k_1{}^{i}\mathrm{d}B'_1 &= 0,\\
-\lambda({}^{i}k_1^2 + {}^{i}\alpha^2{}_1){}^{i}\mathrm{d}A_1 + \left(\lambda'({}^{i}k_1^2 - {}^{i}\alpha'^2_1) - 2\mu'{}^{i}\alpha'^2{}_1\right){}^{i}\mathrm{d}A'_1 + 2i\mu'{}^{i}k_1{}^{i}\beta'_1{}^{i}\mathrm{d}B'_1 &= 0,\\
-2i\mu'{}^{i}k_1{}^{i}\alpha'_1{}^{i}\mathrm{d}A'_1 + \mu'({}^{i}k_1^2 + {}^{i}\beta'^2{}_1){}^{i}\mathrm{d}B'_1 &= 0;
\end{aligned}
\tag{5.22}
$$

order two,

$$
\begin{aligned}
&-\lambda({}^{i}k_2^2+{}^{i}\alpha_2^2)\left({}^{i}\mathrm{d}A_{12}\cos{}^{i}\alpha_2 H+{}^{i}\mathrm{d}A_{22}\sin{}^{i}\alpha_2 H\right)=-i\cot{}^{i}\alpha_1 H{}^{i}\alpha_1{}^{i}\mathrm{d}A_{11}\mathrm{d}H_1,\\
&{}^{i}\alpha_2^{i}\mathrm{d}A_{22}-{}^{i}\alpha'_2{}^{i}\mathrm{d}A'_2+i{}^{i}k_2{}^{i}\mathrm{d}B'_2=-i{}^{i}\alpha_1^{2i}\mathrm{d}A'_1\mathrm{d}H_1+{}^{i}\alpha_1'^{2i}\mathrm{d}A'_1\mathrm{d}H_1-k_{s1}{}^{i}\mathrm{d}B'_1\mathrm{d}H_1\\
&-{}^{i}k_1k_{s1}{}^{i}\mathrm{d}A'_1\mathrm{d}H_1-\lambda({}^{i}k^2{}_2+{}^{i}\alpha^2{}_2)^{i}\mathrm{d}A_{11}+\left(\lambda'({}^{i}k_2^2-{}^{i}\alpha'^2_2)-2\mu'^{i}\alpha'^2{}_2\right){}^{i}\mathrm{d}A'_2\\
&+2i\mu'^{i}k_2{}^{i}\beta'_2{}^{i}\mathrm{d}B'_2=+\lambda'({}^{i}k^2{}_1-{}^{i}\alpha^2{}_1)^{i}\alpha_1{}^{i}\mathrm{d}A_{21}\mathrm{d}H_1+i{}^{i}k_1({}^{i}k_1+k_{s1})^{i}\alpha_1{}^{i}\mathrm{d}A'_1\mathrm{d}H_1\\
&+i\lambda'^{i}\alpha'^3_1{}^{i}\mathrm{d}A_1\mathrm{d}H_1+2i\mu' i({}^{i}k_1+k_{s1})^{i}\beta'^2_1{}^{i}\mathrm{d}B'_1\mathrm{d}H_1,\\
&-2\mu'^{i}\alpha'_2{}^{i}k_2{}^{i}\mathrm{d}A'_2+\mu'\ ({}^{i}k_2^2-{}^{i}\beta'^2_2)^{i}\mathrm{d}B'_2=-2i\mu'^{i}\alpha'^2(k_1+k_{s1})^{i}\mathrm{d}A'_1\mathrm{d}H_1\\
&-2i\mu'^{i}\beta^{2i}\mathrm{d}B'_1\mathrm{d}H_1-2i\mu'^{i}k_1{}^{i}\beta'({}^{i}k_1+k_{s1})^{i}\mathrm{d}B'_1\mathrm{d}H_1;
\end{aligned}
\tag{5.23}
$$

order three,

$$
\begin{aligned}
&-\lambda\left({}^{i}k_3^2+{}^{i}\alpha_3^2\right)\left({}^{i}\mathrm{d}A_{13}\cos{}^{i}\alpha_3 H+{}^{i}\mathrm{d}A_{23}\sin{}^{i}\alpha_3 H\right)=-i\cot{}^{i}\alpha_2 H{}^{i}\alpha_2{}^{i}\mathrm{d}A_{12}\mathrm{d}H_1,\\
&{}^{i}\alpha_3{}^{i}\mathrm{d}A_{23}+i{}^{i}k_3{}^{i}\mathrm{d}B'_3-i{}^{i}\alpha'_3{}^{i}\mathrm{d}A'_3={}^{i}\alpha_1^{2i}\mathrm{d}A_{21}\mathrm{d}H_2+{}^{i}\alpha_2^{2i}\mathrm{d}A_{22}\mathrm{d}H_1+{}^{i}\alpha_1'^{2i}\mathrm{d}A'^2_1\mathrm{d}H_2\\
&\quad+{}^{i}\alpha'^{2i}_2\mathrm{d}A'_2\mathrm{d}H_1+{}^{i}k_1{}^{i}\beta_1{}^{i}\mathrm{d}B'_1\mathrm{d}H_2+{}^{i}k_1k_{s1}{}^{i}\mathrm{d}A_{21}\mathrm{d}H_1+i{}^{i}k_1{}^{i}\alpha_1k_{s1}{}^{i}\mathrm{d}A_{11}\mathrm{d}H_2\\
&\quad-ik_{s1}^2{}^{i}\beta_1{}^{i}\mathrm{d}B'_1{}^{i}\mathrm{d}H_1{}^{i}dH_1+{}^{i}\beta'_1k_{s2}{}^{i}\mathrm{d}B'_1\mathrm{d}H_2+{}^{i}\beta'_2k_{s1}{}^{i}\mathrm{d}B'_2\mathrm{d}H_1,\\
&-\lambda\left({}^{i}k_3^2+{}^{i}\alpha_3^2\right){}^{i}\mathrm{d}A_{13}+\left(\lambda'\left({}^{i}k_3^2-{}^{i}\alpha'^2_3\right)-2\mu'^{i}\alpha'^2_3\right){}^{i}\mathrm{d}A'_3+2i\mu'^{i}k_3{}^{i}\beta'_3{}^{i}\mathrm{d}B'_3\\
&\quad=-i\lambda^{i}k_1^{2i}\alpha_1^{3i}\mathrm{d}A_{21}\mathrm{d}H_2-i\lambda^{i}k_2^{2i}\alpha_2^{3i}\mathrm{d}A_{22}\mathrm{d}H1+i\lambda'^{i}k_1({}^{i}k_1+k_{s2})^{i}\alpha'_1{}^{i}\mathrm{d}A'_{11}\mathrm{d}H_{s2}\\
&\quad+i\lambda'^{i}k_2({}^{i}k_2+k_{s2})^{i}\alpha'^{i}_2\mathrm{d}A'_{21}\mathrm{d}H_1-2i\mu'^{i}\alpha'^{2i}_1\mathrm{d}A'_1\mathrm{d}H_2-2\mu'^{i}\alpha'^{2i}_2\mathrm{d}A'_2\mathrm{d}H_1\\
&\quad+2i\mu'^{i}\beta'^2{}_1({}^{i}k_1+k_{s2})^{i}\mathrm{d}B'_1\mathrm{d}H_2+2i\mu'^{i}k_2^{i}\beta'^{2i}_2\mathrm{d}B'_2\mathrm{d}H_1,\\
&-2i\mu'^{i}\alpha'_3{}^{i}k_3{}^{i}\mathrm{d}A'_3+\mu'({}^{i}k^2{}_3+{}^{i}\beta'^2_3)^{i}\mathrm{d}B'_3=2\mu'^{i}\alpha'^2_2({}^{i}k_{2s}+k_{s1})^{i}\mathrm{d}A'_2\mathrm{d}H_1\\
&\quad+2\mu'^{i}\alpha'^2_1({}^{i}k_1+k_{s2})^{i}\mathrm{d}A'_1\mathrm{d}H_2-i\mu'^{i}\beta'^{3i}\mathrm{d}B'_1\mathrm{d}H_2-i\mu'^{i}\beta'^{3i}\mathrm{d}B'_1\mathrm{d}H_1\\
&\quad-i\mu'^{i}k_2({}^{i}k_2+k_{s1})^{i}\beta'_2\mathrm{d}B'_2\mathrm{d}H_1-i\mu'^{i}k_1({}^{i}k_1+k_{s2})^{i}\beta'_1\mathrm{d}B'_1\mathrm{d}H_2\\
&\quad-i\lambda'^{i}\alpha'^2k_{s1}{}^{i}\mathrm{d}A'_1\mathrm{d}H_1^2-i{}^{i}k_2^2k_{s1}{}^{i}\mathrm{d}A'_2\mathrm{d}H_1-i\lambda'^{i}k_1^2k_{s2}{}^{i}\mathrm{d}A'_2\mathrm{d}H_2\\
&\quad-2i\mu'^{i}\alpha'_1{}^{i}k_1k_{s1}{}^{i}\mathrm{d}A'_1\mathrm{d}H_1\mathrm{d}H_1-2\mu'^{i}k_1{}^{i}\beta'_1k_{s1}{}^{i}\mathrm{d}B'_1\mathrm{d}H_1\mathrm{d}H_1\\
&\quad-2i\mu'^{i}k_2k_{s1}{}^{i}\beta'_2{}^{i}\mathrm{d}B'_2\mathrm{d}H_1-2i\mu'\ ({}^{i}k_1+k_{s1})^{i}k_1{}^{i}\beta'_1{}^{i}\mathrm{d}B'^2_1\mathrm{d}H_1\\
&\quad-2i\mu'^{i}k_1{}^{i}\beta'_1k_{s2}{}^{i}\mathrm{d}B'_1\mathrm{d}H_2.
\end{aligned}
\tag{5.24}
$$

Equations (5.22) describe the conditions to be satisfied by the acoustic-gravity–Scholte wave field following an instantaneous excitation, such as that due to a heavy gust of wind. The interaction of this wave field with the seafloor non-uniformity then forces the second-order acoustic-gravity–Scholte wave field as described by (5.23). The interactions of the first- and second-order wave fields with the seafloor non-uniformity then produce a third-order wave field, and so forth. The entire wave field in the ocean–seafloor coupled system is described by the summation of the solutions to (5.22)–(5.24) and other higher-order solutions. The free wave field includes the order-one natural modes and the response to interactions between free acoustic-gravity waves and seafloor non-uniformity.

The left-hand sides of the three equations (5.22)–(5.24) are linear, and the excitation terms on the right-hand sides of (5.23) and (5.24) contain quantities known from solutions

at the previous order. Equations (5.22)–(5.24) can be expressed in matrix form as

$$\begin{aligned} \boldsymbol{D}_1 \mathbf{d}\boldsymbol{A}_1 &= 0, \\ \boldsymbol{D}_2 \mathbf{d}\boldsymbol{A}_2 &= \mathbf{d}\boldsymbol{F}_2, \\ \boldsymbol{D}_3 \mathbf{d}\boldsymbol{A}_3 &= \mathbf{d}\boldsymbol{F}_3. \end{aligned} \tag{5.25}$$

In (5.25), $\mathbf{d}\boldsymbol{F}_2$ and $\mathbf{d}\boldsymbol{F}_3$ denote the terms on the right-hand sides of (5.23) and (5.24), respectively. These excitation terms represent how lower-order solutions force higher-order effects. In the absence of excitation at the free surface, the first of (5.25) has a non-trivial solution when the determinant of $\boldsymbol{D}_1$ vanishes, or

$$\|\boldsymbol{D}_1\| = 0. \tag{5.26}$$

The free-wave acoustic-gravity–Scholte wave field is any wave field that satisfies (5.26), which in full form can be written as

$$\begin{vmatrix} -\lambda\left({}^{i}k_1^2 + {}^{i}\alpha_1^2\right) & -\lambda\left({}^{i}k_1^2 + {}^{i}\alpha_1^2\right) & 0 & 0 \\ \cos {}^{i}\alpha_1 H & \sin {}^{i}\alpha_1 H & & \\ 0 & {}^{i}\alpha_1 & -{}^{i}\alpha_1 & i^{i}k_1 \\ -\lambda\left(k^2 + \alpha^2\right) & 0 & \left(\lambda'\left({}^{i}k_1^2 - {}^{i}\alpha_1'^2\right) - 2\mu'^{i}\alpha_1'^2\right) & 2i\mu'^{i}k_1{}^{i}\beta'_1 \\ 0 & 0 & -2i\mu'^{i}k_1{}^{i}\alpha'_1 & \mu'\left({}^{i}k_1^2 + {}^{i}\beta_1'^2\right) \end{vmatrix} = 0. \tag{5.27}$$

The condition in (5.27) leads to the dispersion relations for the ith mode, and can be expressed in the form

$$\tan {}^{i}\alpha_1 H = \frac{{}^{i}\alpha_1\left({}^{i}A\,{}^{i}D - {}^{i}B\,{}^{i}C\right)}{\lambda\gamma_1^2\left(\alpha'^{i}D - i^{i}k_1{}^{i}C\right)}, \tag{5.28}$$

where

$$\begin{aligned} &{}^{i}A = \lambda'({}^{i}k_1^2 - {}^{i}\alpha_1'^2) - 2\mu'^{i}\alpha_1'^2, \quad {}^{i}B = 2i\mu'^{i}k_1{}^{i}\beta'_1, \\ &{}^{i}C = 2i^{i}k_1{}^{i}\alpha'_1, \quad {}^{i}D = {}^{i}k_1^2 + {}^{i}\beta_1'^2. \end{aligned} \tag{5.29}$$

Equations (5.28) and (5.29) define the dispersion relations for the fundamental and higher modes represented by $(\cos\alpha H, \sin\alpha H)$, $(\cos 2\alpha H, \sin 2\alpha H)$ and so forth. These dispersion relations assume an undisturbed sea surface. Together with (5.17), they relate the horizontal and vertical wavenumber components to the angular frequency of the free wave acoustic-gravity–Scholte wave field supported by the coupled ocean-water column and seafloor system. The dispersion relations are discussed further in § 7.

The first term on the right-hand side of the first of (5.23) contains a product ${}^{i}\mathrm{d}A_{11}\mathrm{d}H_1$ which represents a second-order interaction between an acoustic-gravity wave and the seafloor. The case studied here is where an acoustic-gravity wave of mode one (i.e. $i = 1$) interacts with the seafloor to excite a mode 2 resonance in the second-order acoustic-gravity wave field according to

$$\begin{aligned} {}^{1}\boldsymbol{k}_1 + \boldsymbol{k}_s &= {}^{2}\boldsymbol{k}_2, \\ \omega + 0 &= \omega. \end{aligned} \tag{5.30}$$

Modes 1 and 2 here refer to the first two modes of the dispersion relation. For waves propagating in a single direction normal to the seafloor contours,

$$\begin{aligned} {}^1k_1 - k_s &= {}^2k_2, \\ \omega + 0 &= \omega. \end{aligned} \tag{5.31}$$

Such a resonance is found to occur at $f = 0.03$ Hz for the present set of seafloor properties and water depth. Here $\mathrm{d}H_1$ for a sloping seafloor equals the Fourier transform derived in § 2:

$$\mathrm{d}H_1(k_s) = F_s(k_s). \tag{5.32}$$

The wavenumber–frequency spectrum for the excitation due to this interaction can be derived as

$$\begin{aligned} S_{AH}({}^2\boldsymbol{k}_2, \omega) &= \left[i\,{}^1\mathrm{d}A_{11}({}^1\boldsymbol{k}_1, \omega)\mathrm{d}H_1(\boldsymbol{k}_s)\right]\left[-i\,{}^1\mathrm{d}A^*_{11}({}^1\boldsymbol{k}_1, \omega)\mathrm{d}H^*_1(\boldsymbol{k}_s)\right], \\ &= S_A({}^1\boldsymbol{k}_1, \omega)S_f(\boldsymbol{k}_s), \quad S_f(\boldsymbol{k}_s) = \overline{F}_s(k_s)\overline{F}^*_s(k_s). \end{aligned} \tag{5.33}$$

The calculation result for the $f = 0.11$ Hz case is discussed in § 8.

6. Forced wave generation

An energetic forced wave field is generated whenever one or more of the nonlinear wave interaction mechanisms above excites the water column–seafloor system into resonance. The analysis below largely is based on the method of Hasselmann (1963) as applied with some extensions (Korde 2024). A forced acoustic-gravity wave field would add a free-surface disturbance according to the term $g\alpha\Gamma$ (Bondi 1947; Abdolali & Kirby 2017), but is neglected because it has only a small effect within the frequency range of interest here (see Appendix A.1).

In the present situation, resonance may be excited by (i) nonlinear interaction between surface waves and the seafloor; (ii) difference-frequency waves arising from quadratic interaction between two closely spaced frequencies interacting with the seafloor; (iii) nonlinear interaction between surface waves, their reflections from the shore and the seafloor; (iv) acoustic-gravity waves interacting with the sloping seafloor. The forcing spectrum $S_E(\boldsymbol{k}, \omega)$ can be derived independently in each case, and they may act concurrently. In the case of direct linear forcing, if the pressure amplitudes are large enough to begin with, it is not as critical for the forcing wave field to excite an acoustic-gravity wave resonance as in the case of second-order wave–wave and wave–seafloor interactions for which energy transfer from the second-order effects to the acoustic-gravity wave field reaches a local maximum in the wavenumber–frequency domain at each resonance.

Here, the excitation is applied to the lowest order of the perturbation expansion. The forced-wave wavenumber spectrum $S_A(\boldsymbol{k}, t)$ is given by (Korde 2024)

$$S_A(\boldsymbol{k}, t)\Big|_{DS} = \frac{\pi t^i D_1^2}{2\omega_1^2} S_E(\omega_1, \boldsymbol{k})\Big|_{DS}. \tag{6.1}$$

Here DS represents a dispersion surface, S_E denotes the forcing spectrum causing resonance and ${}^iD_1$ for mode i order-one for depth H for excitation on the surface $\zeta = 0$ is

$${}^iD_1 = \frac{2\left[\sin {}^i\alpha_1 H + f_1(1 - \cos {}^i\alpha_1 H)\right]}{\rho^i\alpha_1 H(1 + f_1^2)}. \tag{6.2}$$

Here, $f_1 = -\cot\alpha_1 H$ for mode i. For a surface-wave frequency spectrum $S_e(\sigma)$ with the wave-elevation amplitude $\mathrm{d}Z(\sigma)$ and a reflection coefficient from shore C_{SR} (assumed to be frequency-independent as a simplification), the excitation spectrum $S_E(\omega_1)$ can be written as

$$S_E(\omega_1) = C_{SR} S_e(\sigma), \quad \omega_1 = \sigma + \sigma, \boldsymbol{k} = \boldsymbol{\kappa} + \boldsymbol{\kappa}, \quad k = \kappa - \kappa = 0. \tag{6.3}$$

The acoustic-gravity wave field in this case is purely vertical and there is no propagation in the horizontal direction. In shallow water, resonance is possible only for modes $i \geqslant 3$, which undergo more scattering (Hasselmann 1963), and thus are not studied further here.

For acoustic-gravity wave interacting with the sloping seafloor with $S_{AH}(\boldsymbol{k}, \omega)$, the Fourier coefficient is

$$\mathrm{d}S_{AH}(\boldsymbol{k}, t) = \sqrt{S_{AH}(\boldsymbol{k}, t)\mathrm{d}\boldsymbol{k}}. \tag{6.4}$$

Thus

$$S_E({}^2\boldsymbol{k}, t) = S_{AH}({}^1\boldsymbol{k}, t) S_f(\boldsymbol{k}_s), \quad {}^2\boldsymbol{k} = {}^1\boldsymbol{k} + \boldsymbol{k}_s. \tag{6.5}$$

The excitation of acoustic-gravity and Scholte waves by the interaction of surface waves with the sloping seafloor needs a different approach. It follows from (2.30)–(2.32) that this interaction excites the acoustic-gravity–Scholte wave field from the seafloor. Further, the excitation is applied to the lowest-order system in (5.22). Hence, the forced system can be described as

$$\begin{aligned}
-\lambda({}^i k_1^2 + {}^i\alpha_1^2)\left({}^i\mathrm{d}A_{11}\cos{}^i\alpha_1 H + {}^i\mathrm{d}A_{21}\sin{}^i\alpha_1 H\right) &= 0,\\
{}^i\alpha_1^i\mathrm{d}A_2 - {}^i\alpha'_1{}^i\mathrm{d}A'_1 + i^i k_1{}^i\mathrm{d}B'_1 &= 0,\\
-\lambda({}^i k_1^2 + {}^i\alpha^2{}_1)^i\mathrm{d}A_1 + \left(\lambda'({}^i k_1^2 - {}^i\alpha'^2_1) - 2\mu'^i\alpha'^2{}_1\right){}^i\mathrm{d}A'_1 + 2i\mu'^i k_1{}^i\beta'_1{}^i\mathrm{d}B'_1 &= \mathrm{d}P,\\
-2i\mu'^i k_1{}^i\alpha'_1{}^i\mathrm{d}A'_1 + \mu'({}^i k_1^2 + {}^i\beta'^2{}_1)^i\mathrm{d}B'_1 &= 0.
\end{aligned} \tag{6.6}$$

For forced-wave solutions that lie on the dispersion surfaces for mode one, (5.22) can be used to express $\mathrm{d}A_{21}$, $\mathrm{d}A'$ and $\mathrm{d}B'$ in terms of $\mathrm{d}A_{11}$ (Korde 2024), Defining

$$\begin{aligned}
A &= \lambda'(k_1^2 - \alpha'^2_1) - 2\mu'\alpha'^2_1, \quad B = 2i\mu' k_1\beta'_1,\\
C &= 2i\mu' k_1\beta'_1, \quad D = \mu'(k_1^2 + \beta'^2_1),
\end{aligned} \tag{6.7}$$

and

$$\begin{aligned}
f_0 &= -\lambda(k_1^2 + \alpha_1^2), \quad f_1 = -\cot\alpha_1 H,\\
f_2 &= -\frac{\alpha_1}{\alpha' - ikC/D} f_1, \quad f_3 = -\frac{C}{D} f_2,
\end{aligned} \tag{6.8}$$

the third of (6.6) can be written as

$$(f_0 + Af_2 + Bf_3)\mathrm{d}A_{11} = \mathrm{d}P. \Rightarrow \mathrm{d}A_{11} = \left(\frac{1}{f_0 + Af_2 + Bf_3}\right)\mathrm{d}P. \tag{6.9}$$

Both $\mathrm{d}P$ and $\mathrm{d}A$ are the Fourier coefficients at each (k, ω), and f_0, f_1 and f_2 also are functions of k and ω. Denoting the wavenumber as a vector to allow for directionality, $S_E(\boldsymbol{k}, t)$ can be expressed as

$$S_E(\boldsymbol{k}, t) = \frac{S_{P_\Delta}(\boldsymbol{k}, t)}{(f_0 + Af_2 + Bf_3)^2}, \tag{6.10}$$

so that,

$$S_A(\boldsymbol{k}, t) = \frac{\pi t D_f^2}{2\omega^2} S_E(\boldsymbol{k}, t), \quad \omega = \sigma. \tag{6.11}$$

Here

$$D_f = \frac{1}{(f_0 + Af_2 + Bf_3)}. \tag{6.12}$$

When the forcing mechanism acts on the surface $\zeta = 0$, and hence, $S_E(\boldsymbol{k}, t) = S_{PS}(\boldsymbol{k}, t)$ (see (4.8)) so that

$$S_A({}^2\boldsymbol{k}, t) = \frac{\pi t^1 D_1^2}{2\omega^2} S_E(\boldsymbol{k}, t). \tag{6.13}$$

The evolution equation for $S_A(\boldsymbol{k}, t)$ (using $i = 1$ for example) can be written as (assuming stationarity of the surface-wave field) (Whitham 1973)

$$\frac{\mathrm{d}S_A(\boldsymbol{k}, t)}{\mathrm{d}t} = \frac{\pi D_j^2}{2\omega_1^2} S_E(\omega_1, \boldsymbol{k}) - \frac{S_A}{t}. \tag{6.14}$$

Here $D_j = D_1$ or D_f depending on the source of excitation. Interactions with bottom sediment, for example the formation of seafloor ripples, can cause dissipation (Arduin *et al.* 2002). Using a damping rate of c_t to include energy dissipation in the seafloor and (to a smaller extent) within the water layer,

$$\frac{\mathrm{d}S_A(\boldsymbol{k}, t)}{\mathrm{d}t} = \frac{\pi D_1^2}{2\omega_1^2} S_E(\omega_1, \boldsymbol{k}) - \frac{S_A}{t} - c_t S_A. \tag{6.15}$$

If the interaction time is denoted as t_e (Korde 2024), the wavenumber spectrum at the present time $t > t_e$ can be found as

$$S_A(\boldsymbol{k}, t) = \int_0^{t_e} \frac{\pi D_1^2}{2\omega^2} S_E(\boldsymbol{k}, \tau)\mathrm{d}\tau - \int_0^{t} \left(\frac{1}{\tau} + c_t\right) S_A(\boldsymbol{k}, \tau)\mathrm{d}\tau. \tag{6.16}$$

If $t \leqslant t_e$, then the upper limit on the first integral in (6.16) would change to t. For a wave group propagating through the interaction region, $t > t_e$ means the group has moved out of the interaction region and is not being amplified further. With $\gamma = \omega/c_1 = \sqrt{k^2 + \alpha^2}$, the wavenumber spectrum $S_P(\boldsymbol{k})$ for the pressure variation in the water column is (Korde 2024)

$$S_P(\boldsymbol{k}, t) = \frac{\mathrm{d}P_1 \mathrm{d}P_1^*}{\mathrm{d}\boldsymbol{k}} = \left(\lambda\gamma^2\right)^2 S_A(\boldsymbol{k}, t). \tag{6.17}$$

The wavenumber spectrum (convertible to a frequency spectrum) for the power density is then

$$S_W(\boldsymbol{k}, t) = \frac{S_P(\boldsymbol{k}, t)}{\rho c_1}. \tag{6.18}$$

The power density for the group $(\boldsymbol{k}, \omega)$ at the seafloor can be found using

$$\Pi(\boldsymbol{k}, t) = \sqrt{S_W(\boldsymbol{k}, t)\mathrm{d}\boldsymbol{k}}, \tag{6.19}$$

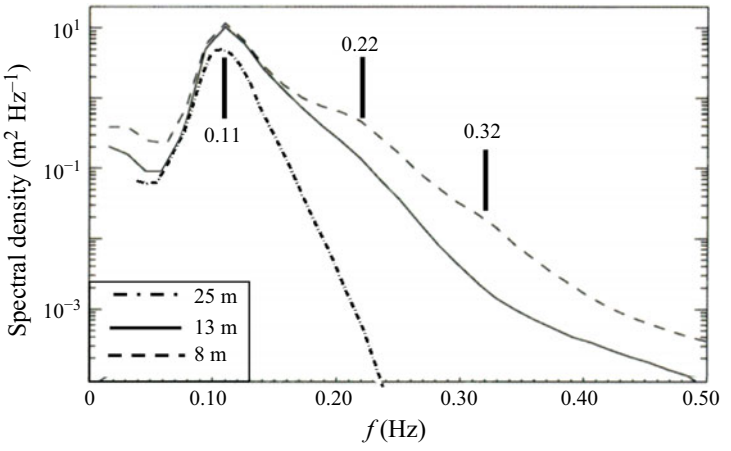

Figure 2. Power spectral density versus frequency for bottom pressure observed in 25- (dash–dotted curve), 13- (solid curve) and 8- (dashed curve) m water depth offshore of the Outer Banks of North Carolina during a 'nor'easter' storm on 26 October1990. Significant wave height (four times the standard deviation of sea-surface fluctuations) was 5 m in 25 m water depth (from Elgar *et al.* (1995)).

where Π is in units such as watts per square metre. The pressure amplitudes at the seafloor are given by the Fourier coefficients $\mathrm{d}P$ as

$$|\mathrm{d}P| = \sqrt{S_P(\boldsymbol{k}, t)\mathrm{d}\boldsymbol{k}}, \;\; \mathrm{d}\boldsymbol{k} = \mathrm{d}k_1\mathrm{d}k_2. \tag{6.20}$$

The wavenumber spectrum for the Scholte waves forming part of this group and the Scholte wave Fourier coefficients are given by

$$\begin{aligned} S_R(\boldsymbol{k}, t) &= \left[\gamma_p^2 F_2(\boldsymbol{k}, \alpha, \alpha', \beta) + \gamma_s^2 F_3(\boldsymbol{k}, \alpha, \alpha', \beta')\right] \frac{\mathrm{d}A_1 \mathrm{d}A_1^*}{d|\boldsymbol{k}|\mathrm{d}\omega} \\ &= \omega^2 \left[\frac{F_2(\boldsymbol{k}, \alpha, \alpha', \beta')}{c_p^2} + \frac{F_3(\boldsymbol{k}, \alpha, \alpha', \beta')}{c_s^2}\right] S_A(\boldsymbol{k}, t), \\ |\mathrm{d}R| &= \sqrt{S_R(\boldsymbol{k}, t)\mathrm{d}\boldsymbol{k}}, \end{aligned} \tag{6.21}$$

where $\mathrm{d}R$ represents the Fourier coefficient for the Scholte-wave displacement amplitudes. Here, for mode one and order one,

$$F_2(\boldsymbol{k}, \alpha, \alpha', \beta') = f_2 f_2^*, \quad F_3(\boldsymbol{k}, \alpha, \alpha', \beta') = f_3 f_3^*, \tag{6.22}$$

where f_2 and f_3 are as defined in (6.8).

7. Results

The frequency variations of observed spectral densities (figure 2) suggest that one source of pressure amplification at low frequencies ($f = 0.01$, 0.02 and 0.03 Hz) in 13 and 8 m depth may be quadratic interactions between surface waves near 25 m depth. Of particular interest here is whether difference-frequency waves arising in ∼25 m depth could interact with the seafloor to produce acoustic-gravity–Scholte waves in the shoreward direction. In addition to the nonlinear interaction between shoreward waves and the seafloor, other types of nonlinear interaction studied here include shoreward surface waves interacting with reflected-surface-waves to generate a surface wave that interacts nonlinearly with the seafloor, and acoustic-gravity waves interacting with the seafloor. In all cases, the

Property	Value (units)
Density ρ'	1.8×10^3 kg m^{-3}
Lamé constant λ'	1.365×10^{10} N m^{-2}
Lamé constant μ'	1.67×10^{10} N m^{-2}
Poisson ratio ν	0.225
Bulk modulus K	2.48×10^{10} N m^{-2}
Dilatational wave c_p	5.11×10^3 m s^{-1}
Shear wave c_s	3.05×10^3 m s^{-1}

Table 1. Seafloor density and elastic constants used in the calculations (estimates based on Turgut & Yamamoto (1990)).

main interest is in estimating the bottom pressures and power densities associated with the resulting acoustic-gravity–Scholte wave fields, and in some cases also the Scholte-wave amplitudes.

There is spatial and temporal variability in the seafloor stratigraphy on the North Carolina inner shelf (Meisburger, Judge & Williams 1989), and the surface waves decay exponentially with depth, and thus a single layer of the seafloor with depth-averaged properties is considered. The seafloor is assumed to be comprised of a saturated porous mix of coarse to densely packed sand and silt interspersed with water particles. The properties of this layer were derived using densities and bulk moduli obtained from the literature (Turgut & Yamamoto (1990), table I), allowing that the storm conditions would drive greater amounts of water into the porous seafloor. The mechanical properties and the dilatational and distortional phase velocities computed from them are estimated using the law of mixtures (table 1). As an example of the approximate calculations, $\lambda' = 0.5\lambda_s + 0.5\lambda$, given $K_s = \lambda_s + (2/3)\mu_s$, and $\nu_s = 0.5\lambda_s/(\lambda_s + \mu_s)$, where the bulk modulus K_s and Poisson ratio ν_s for sand particles are, respectively, 3.6×10^{10} N m^{-2}, and $\nu_s = 0.3$. The acoustic phase velocity in seawater $c_1 = 1.5 \times 10^3$ m s^{-1}, and the seawater bulk modulus (equal to the Lamé constant λ) is 2.6×10^9 N m^{-2}. The dissipation-attenuation coefficients for frequencies ~ 0.01 Hz were $c_{t1} = 1.0 \times 10^{-4}$ m^2 Hz^{-1}m^{-1} for the seafloor, and $c_{t2} = 1.0 \times 10^{-6}$ m^2 Hz^{-1}m^{-1} for seawater. The dissipation constants for propagation of the acoustic-gravity waves over the seafloor (Kibblewhite 1989) were obtained from previous field observations, while for propagation through water (figure 5 in Gottwald (1970)) these are derived empirically from published data. In both cases, the dissipation coefficients were assumed to be averaged over frequency. Water depths at the sensor locations (figure 1) were measured. The effect of uncertainties in the seafloor elastic parameters, dissipation coefficients, and the water depth are examined in Appendix A.

In the dispersion relations derived here, the phase velocity of the Scholte waves is computed as $c_R = \omega/k$. The phase velocity of the Rayleigh wave on dry ground onshore of the beach is estimated according to $c_{Rg} = c_{sg}(0.87 + 1.12\nu_g)/(1 + \nu_g)$, with the shear-wave velocity on dry ground $c_{sg} = 2.8 \times 10^3$ m s^{-1}, and the Poisson ratio of dry ground $\nu_g = 0.25$ (Graff (1991), chapter 6). Although the storm system exciting surface-wave–seafloor, and surface-wave–surface-wave–seafloor interactions likely lasted longer (Herbers & Guza 1994), the calculations here are stopped at $t = 60$ hr.

Bottom pressures observed during the storm were estimated from 2.83 hr-long time series obtained midday of 26 Oct 1990 with Setra pressure gages buried 0.1 m below the seafloor to minimize flow noise and sampled at 4 (13 m depth) and 2 (8 m depth) Hz (Herbers & Guza 1994). After subdividing the 2.83 hr records into 1024 s subsections that were tapered with a Hanning window and overlapped 75 %, the spectral estimates

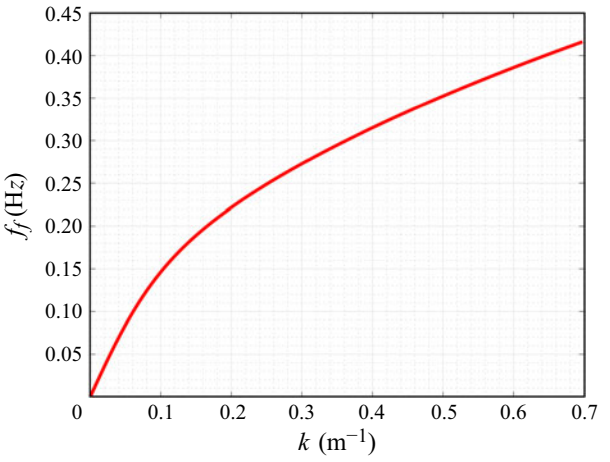

Figure 3. The finite-depth dispersion relationship (frequency f_f versus wavenumber κ) for surface waves in 13 m water depth.

were averaged over 16 frequency bands to produce a frequency resolution of 0.0156 Hz with approximately 320 degrees of freedom. Spectra were averaged over 15 guages in 13 m water depth (250 × 250 m array) and 10 guages in 8 m water depth (200 × 150 m array). The spatial separation of some of the sensors in each array was small relative to a wavelength of the low frequency waves, and thus those estimates are not independent, resulting in approximately 1000 degrees of freedom for the longest wavelengths. In addition, sea-surface elevation spectra were estimated with observations from a buoy (Datawell Waverider) deployed in 25 m water depth offshore of the pressure sensor arrays (figure 1). Three 1 hr records of surface elevation spectra were averaged, and converted to bottom pressure using linear finite depth theory.

For unidirectional waves, frequency spectra can be converted to wavenumber spectra using (Komen & Hasselmann 1996)

$$S_E(\sigma)\mathrm{d}\sigma = \kappa S_E(\kappa)\mathrm{d}\kappa, \tag{7.1}$$

thus,

$$S_E(\kappa) = \frac{S_E(\sigma)}{\kappa}\frac{\mathrm{d}\sigma}{\mathrm{d}\kappa}. \tag{7.2}$$

From linear shallow water wave theory,

$$\frac{\mathrm{d}\sigma}{\mathrm{d}\kappa} = \frac{1}{2}\frac{\sigma}{\kappa}\left(1 + \frac{2\kappa H}{\sinh 2\kappa H}\right). \tag{7.3}$$

Hence,

$$S_E(\kappa) = \left[\frac{1}{2}\frac{\sigma}{\kappa^2}\left(1 + \frac{2\kappa H}{\sinh 2\kappa H}\right)\right] S_E(\sigma). \tag{7.4}$$

8. Discussion of results

For surface waves in constant finite-water depth the dispersion relation is $\sigma^2 = g\kappa \tanh \kappa H$. For $H = 13$ m the $\kappa - \sigma$ relationship increases nonlinearly with κ up to $\kappa \approx 0.3\,\mathrm{m}^{-1}$, after which it becomes approximately linear (figure 3), indicating that the longer waves are more strongly affected by the shallow depth than shorter waves.

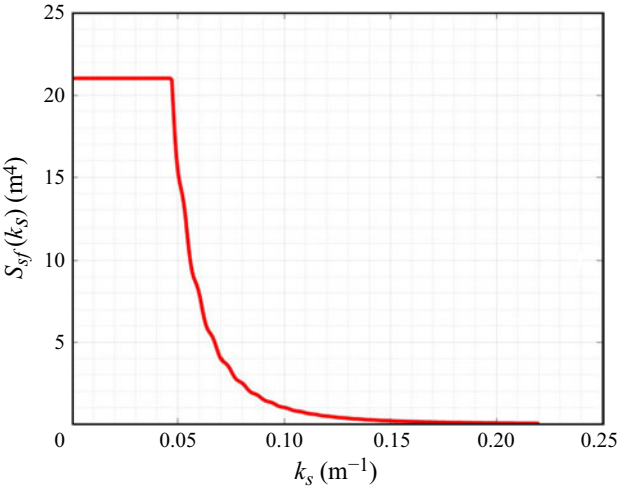

Figure 4. Wavenumber spectral density $S_{sf}(\mathrm{k}_s)$ versus wavenumber k_s for a seafloor profile $h(x) = bx$.

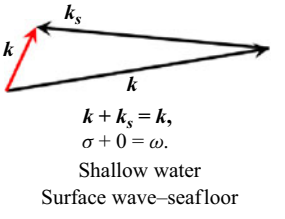

Figure 5. A schematic showing the type of wave–seafloor interaction that potentially could excite a resonant acoustic-gravity–Scholte wave.

The wavenumber spectrum $S_{sf}(k_s)$ for the sloping seafloor evaluated according to (2.25) and (2.26) takes on large values as $k_s \to 0$, and decreases rapidly beyond $k_s \approx 0.05\,\mathrm{m}^{-1}$ (figure 4).

Seafloor interactions with the longer surface waves are more likely to excite resonances of the acoustic-gravity–Scholte wave system (figure 5) given that these waves propagate at acoustic speeds. In this case,

$$\begin{aligned} &\boldsymbol{\kappa} + \boldsymbol{k}_s = \boldsymbol{k}, \\ &\sigma + \sigma_s = \omega, \quad \because \sigma_s = 0, \quad \omega = \sigma. \end{aligned} \tag{8.1}$$

When the surface waves $(\boldsymbol{\kappa}, \sigma)$ propagate shoreward in a direction normal to the depth contours,

$$k = \kappa - k_s; \quad \omega = \sigma. \tag{8.2}$$

The normalized velocities c_R/c_1, where c_R is the phase velocity of the Scholte waves (Hasselmann 1963) dispersion relations for the first three modes of the acoustic-gravity–Scholte wave field decrease rapidly with frequency (normalized by $(\omega H)/(2\pi c_1)$) until normalized frequency is 0.005, and then decrease slowly (figure 6). The resonant frequency–wavenumber combinations here are determined approximately using a numerical scheme. The normalized frequency values for 13 m depth (figure 6) are two orders of magnitude smaller than for 2800 m depth dispersion curves (Korde 2024). The rapid decrease of c_R/c_1 with frequency at low frequencies presents a challenge for the

f_1 (Hz)	κ (m^{-1})	k_s (m^{-1})	f_3 (Hz)	k (m^{-1})
0.01	6.00×10^{-3}	5.94×10^{-3}	0.01	3.5×10^{-5}
0.02	1.12×10^{-2}	1.11×10^{-2}	0.02	7.0×10^{-4}
0.03	1.64×10^{-2}	1.62×10^{-2}	0.03	1.1×10^{-4}

Table 2. Wavenumber and frequency combinations tested for wave–seafloor interaction, with k the vector sum of κ and k_s.

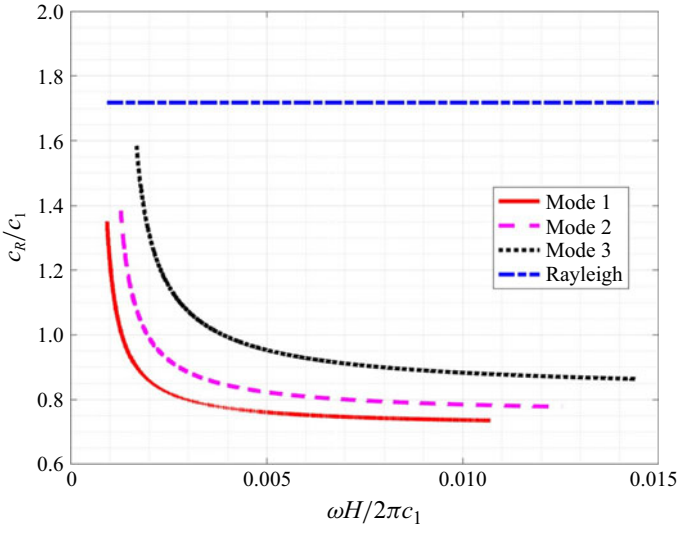

Figure 6. Normalized dispersion relations (normalized phase speed c_R/c_1) versus normalized frequency $(\omega H)/(2\pi c_1)$) for the first three modes of the acoustic-gravity–Scholte wave field and for a Rayleigh wave.

numerical search method used for finding the zeros of the determinant $\boldsymbol{D}_1$ (5.26) in the (k, ω) plane. The mode one curve (figure 6, red curve) is expected to approach the horizontal straight line representing a Rayleigh wave on shore (figure 6, blue dashed line) as $H \to 0$, where the Scholte wave loses the water layer above the seafloor and begins to propagate as a Rayleigh wave on land (cf. Eyov *et al.* (2013) for a similar observation). The dispersion relations derived here strictly apply only when $f \geqslant 0.01$ Hz where the contribution of the gravity term is small (see Appendix A.1) and provide the $(\boldsymbol{k}, \omega)$ combinations for which free-wave solutions for the acoustic-gravity–Scholte system exist.

Resonance occurs when the (k, ω) combinations in (8.1) and (8.2) lie on the dispersion surface for the ith acoustic-gravity–Scholte wave mode. The acoustic-gravity waves in water and the Scholte waves on the seafloor form a wave group, transmitting energy at the group velocity $\mathrm{d}\omega/\mathrm{d}t$ (Korde 2024). For the frequencies shown in table 2, the surface-wave–seafloor interaction leads to resonant excitation of mode $i = 1$. Two sets of results are discussed below: (i) the evolution of propagating resonant wave groups as they travel through the interaction region at a group velocity $C_g = 2.9 \times 10^3$ m s^{-1} over time $t \leqslant t_e$ (see (6.16); (ii) pressure and power density evolutions for a stationary resonant array inside the interaction region.

There are surface-wave frequency and wavenumber combinations in 25 m depth that could produce quadratic interactions leading to difference frequency surface waves (table 3), which then interact with the seafloor to generate acoustic-gravity–Scholte waves.

f_1 (Hz)	f_2 (Hz)	κ_1 (m^{-1})	κ_2 (m^{-1})	$f_1 - f_2$ (Hz)	k_s (m^{-1})	k (m^{-1})
0.11	0.10	0.0560	0.0467	0.01	0.093	3.5×10^{-5}
0.12	0.10	0.0640	0.0467	0.02	0.01723	7.0×10^{-5}
0.13	0.10	0.0723	0.0467	0.03	0.0256	1.1×10^{-4}

Table 3. Quadratic surface-wave interactions in 25 m depth leading to difference-frequency surface waves that interact with the seafloor .

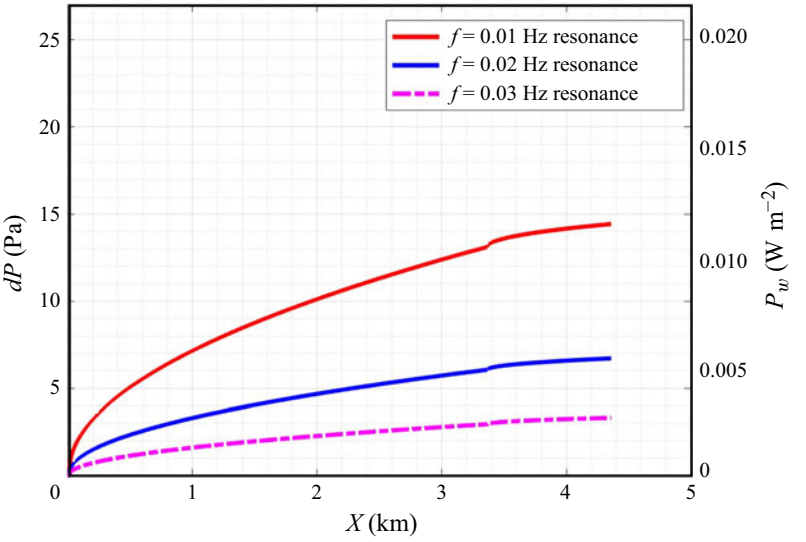

Figure 7. Pressure amplitude (left-hand y-axis) and power density (right-hand y-axis) versus distance from 0 to 4.2 km (from 25 to 8 m water depth) for three resonant acoustic-gravity wave–Scholte wave groups for $f =$ 0.01 (red curve), 0.02 (blue curve) and 0.03 Hz (pink curve).

Resonant acoustic-gravity–Scholte wave groups generated near 25 m depth (i.e. their $(\omega, \boldsymbol{k})$ are on the dispersion surface, in this case for mode $i = 1$) gain energy as they propagate to 8 m water depth (figure 7, with $X = C_g t$). The slight jumps in the curves at $X \sim 3.4$ km are due to a change in the slope of the sea floor at 13 m depth, which changes the amplification rate. The dissipation coefficients used for these calculations are described in § 7. The gains in the Fourier coefficients for pressure in travelling from 25 to 8 m depth are greatest for the wave group that resonates at $f = 0.01$ Hz, $(\omega, k) =$ $(6.28 \times 10^{-2}$ rad s^{-1}, 3.5×10^{-5} m$^{-1})$ (orange curve in figure 7). Seafloor pressure rises approximately 15 Pa during the short travel time from 25 to 8 m depth. Smaller increases are noted for the other wave groups (∼7 Pa and 3 Pa, figure 7). Power gains exhibit a similar trend, with the maximum gain of approximately 0.012 W m^{-2} for the $f = 0.01$ Hz wave group, and 3–5 mW m^{-2} for the other wave groups (corresponding to $f = 0.02$ and 0.03 Hz) (figure 7). The Scholte wave Fourier coefficient for the $f = 0.01$ Hz wave group increases to ∼0.48 µm, and to ∼0.34 and 0.24 µm for the other wave groups (figure 8). These results are obtained for particular combinations of surface wave and seafloor wavenumbers resulting in (k, ω) values that lie on the acoustic-gravity–Scholte wave dispersion surfaces. Other combinations arising from seafloor non-uniformity that lead to resonant interactions are not considered here, but should be studied in future work.

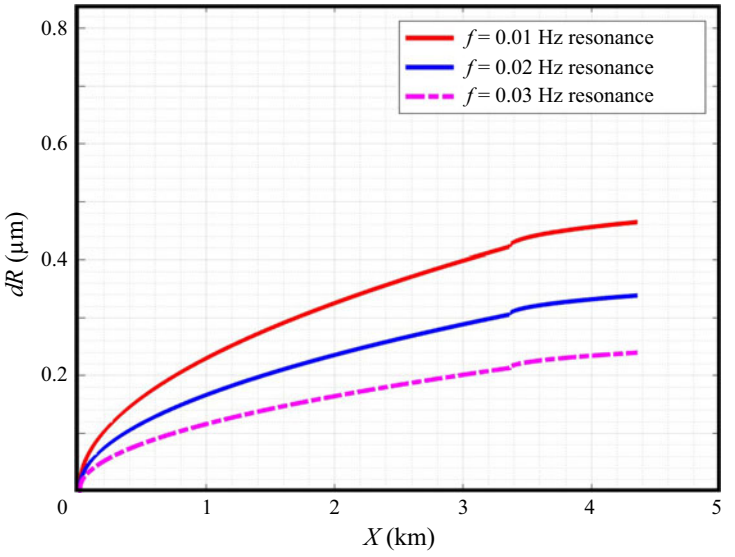

Figure 8. Scholte-wave amplitude versus distance from 0 to 4.2 km (from 25 to 8 m water depth) for three resonant acoustic-gravity wave–Scholte wave groups for $f = 0.01$ (red curve), 0.02 (blue curve) and 0.03 Hz (pink curve).

From the standpoint of utilizing the acoustic-gravity waves to generate energy on the seafloor, it is of interest to estimate the second-order bottom pressures and corresponding power densities available to a stationary array of mutually coupled mechanical oscillators that are distributed over the seafloor between 13 and 8 m depths and tuned to operate at resonance. As the propagating wave groups at particular frequencies travel over the array, resonant oscillations are excited, which can be used for power conversion by electromechanical means. Resonant oscillations and power conversion continue as long as wave groups causing resonance continue to travel over the array. The pressure and power densities incident on and available to a resonant array were estimated over the 3 hr observational period (which is taken to be the period of resonant excitation of the array), neglecting possible attenuation effects of the energy conversion mechanism, and assuming that all of the energy in the waves is available for conversion. The greatest increase in the pressure amplitudes incident on the array (as estimated using (6.16)) is for $f = 0.01$ Hz (approximately 120 Pa over 3 hr, red curve in figure 9), with smaller increases noted at $f = 0.02$ and $f = 0.03$ Hz (40 Pa and 10 Pa, blue and pink curves in figure 9, respectively). Available power density at $f = 0.01$ Hz is approximately 0.10 W m^{-2} at $t = 3$ hr (orange curve in figure 9), with smaller amounts noted at $f = 0.02$ Hz and $f = 0.03$ Hz (0.03 W m^{-2} and 0.01 W m^{-2}, blue and pink curves in figure 9, respectively).

The pressure amplitude and power densities available to the resonant array from interaction of shoreward waves, reflected waves, and the seafloor (table 4) at $f = 0.22$ Hz are 32 Pa and 0.03 W m^{-2}, respectively (figure 10). Pressure and power densities from similar interactions leading to $f = 0.31$ Hz are small (figure 10). The qualitative difference between the results at $f = 0.22$ and 0.31 Hz may be partially due to the decrease in the seafloor contribution $F_s(k_s)$ (figure 4) between the two frequencies, although these results may be sensitive to the choice of interacting frequencies, which requires further investigation. The frequency–wavenumber combinations at the frequencies $f = 0.01$, 0.02, 0.03 and 0.22 Hz lie on the dispersion surface for the first mode for the region between 13

f_1	κ_I	f_2	κ_R	k_s	f_3	k
0.12	7.77×10^{-2}	0.10	6.1×10^{-2}	1.152×10^{-2}	0.22	1.41×10^{-3}
0.16	1.14×10^{-1}	0.15	1.05×10^{-1}	5.94×10^{-3}	0.31	1.99×10^{-3}

Table 4. Wavenumber and frequency combinations tested for wave–wave–seafloor interaction with k the vector sum of κ_I, κ_R, and k_s (frequencies in hertz, wavenumbers in 'per metre').

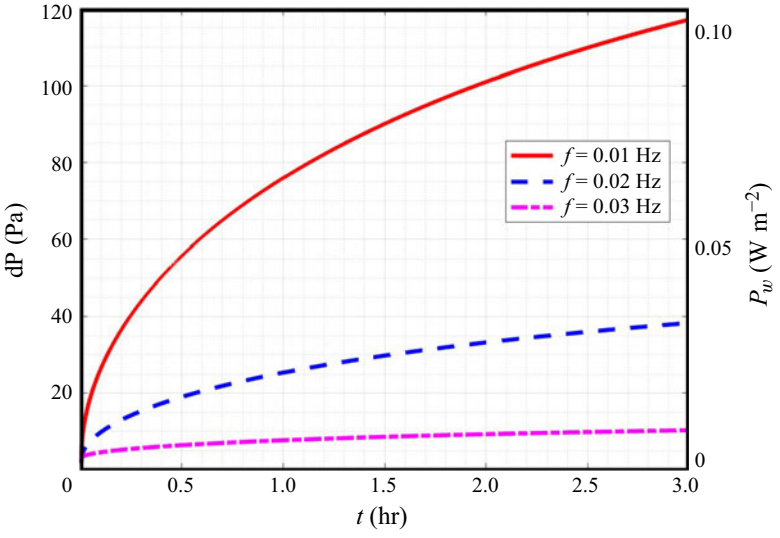

Figure 9. Pressure amplitude (left-hand y-axis) and power density (right-hand y-axis) over a resonant oscillator array between 13 and 8 m depth versus time for the second-order interaction between waves at $f = 0.01$ (red curve), 0.02 (blue curve) and 0.03 Hz (pink curve) and the seafloor.

and 8 m depth, and thus it is expected that a stationary sensor within this region would record a second-order pressure signal that grows with time at resonant frequencies.

A significant amount of energy from first-order pressures also may be available to the oscillator array at the seafloor between 13 and 8 m depths. Various device concepts designed for conversion from first-order effects have been studied (Wang *et al.* 2024). Although a tuneable oscillator array may be capable of utilizing energy from first- and second-order effects, here the interest is in the energy from second-order effects, which, unlike energy from first-order pressures, also is available in deep water (Korde & McBeth 2022).

The excitation spectrum due to surface-wave–seafloor interactions is applied on the first-order dynamics in the perturbation expansion of (5.22). This forcing leads to resonant excitation of acoustic-gravity–Scholte modes, which in turn interact with the sloping seafloor and excite higher-order acoustic-gravity–Scholte waves, as discussed in § 5. Thus, the nonlinear interaction between the mode-one first-order acoustic-gravity wave and the seafloor excites a mode-two second-order acoustic-gravity wave with $f = 0.11$ Hz, with a normalized (by the value in 13 m depth) value 1.4×10^{-4}. Similar interactions in the lower frequency range ($\leqslant f = 0.03$ Hz) are not studied here because of numerical inaccuracies encountered over the low wavenumber range of the dispersion surfaces.

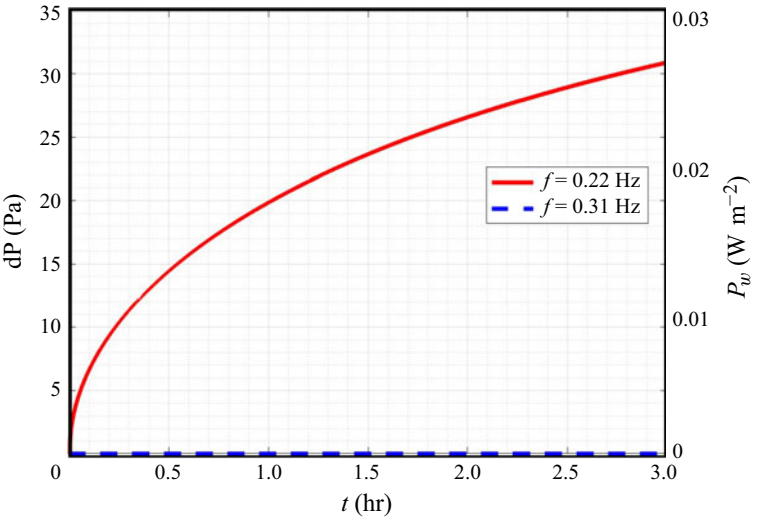

Figure 10. Pressure amplitude (left-hand y-axis) and power density (right-hand y-axis) over a resonant oscillator array between 13 and 8 m depth versus time for the interaction between shoreward waves, reflected waves and the seafloor for $f = 0.22$ (red curve) and 0.31 Hz (blue curve).

The total power density available for conversion at the seafloor at a particular location is the sum total of the power densities in the frequency range over which the surface-wave–seafloor interactions are significant (e.g. in the present case, $f \in (0.01, 0.03)$ Hz). The power density could be greater in stormy weather at nearshore sites where longer swells from distant storms approach frequently, and at sites where the seafloor slope is greater. At some locations, additional power from first-order pressures, wave–wave–seafloor interactions between incident and reflected waves at slightly different frequencies and the sloping seafloor, as well as acoustic-gravity-wave–seafloor interactions also may be available. The power amounts integrated over frequencies and area may be appreciable at some sites and could provide a long-term power source for seafloor and water-column sensors, particularly when adequate energy storage means are provided.

The higher-order effects (figures 9 and 10) would be added to the seafloor pressures due to surface-wave elevations directly overhead in 8 m depth. Additionally, it is expected that similar interactions to those considered here would occur over the ∼1 km of distance between 13 and 8 m water depths. These interactions, in addition to the pressures due to wave elevations in 8 m depth also contribute to the seafloor pressures (and power densities) in 8 m depth. The present results quantify the potential nonlinear mechanisms responsible for a portion of the observed pressure spectra at $H = 8$ m depth (figure 2, from Elgar *et al.* (1995)), while estimating the contributions of acoustic-gravity waves generated by surface-wave nonlinear interactions at $H = 13$ m depth.

The wave–seafloor interactions leading to acoustic-gravity waves at $f = 0.01$, 0.02 and 0.03 Hz reach normalized pressure spectral values in the region between 13 and 8 m depth that are approximately 4.0 %, 0.5 % and 0.1 % of the values in 13 m depth (figure 11).

The wave–wave–seafloor interactions leading to acoustic-gravity waves at $f = 0.22$ and $f = 0.31$ Hz reach normalized pressure spectral values in the region between 13 and 8 m depth, that are approximately 2.0 % and <0.1 % of the values in 13 m depth (figure 12).

Although there was ∼ 40 % loss of energy flux between 13 (wave heights were 5 m) and 8 m (wave heights were 4 m) depth, dissipation of depth-limited breaking waves typically increases as f^2 (Mase & Kirby 1992; Kaihatu & Kirby 1995; Elgar *et al.* 1997), and

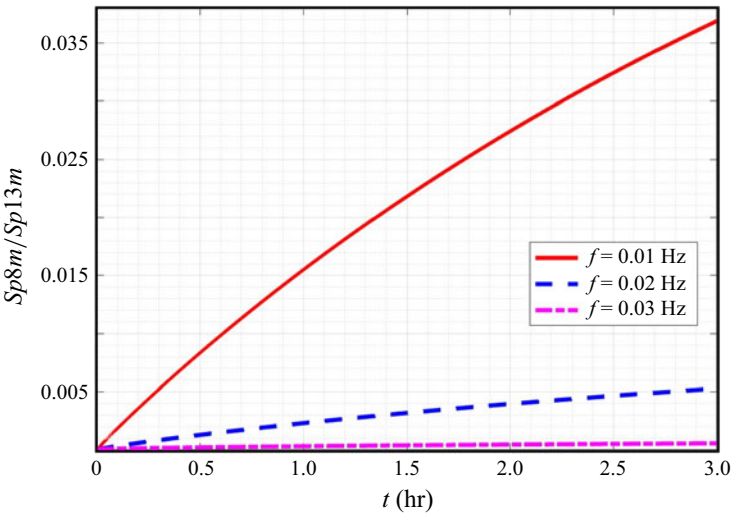

Figure 11. Seafloor pressure Fourier coefficients in 8 m water depth relative to those in 13 m water depth due to wave–seafloor interactions for $f = 0.01$ (red curve), 0.02 (blue curve) and 0.03 Hz (pink curve).

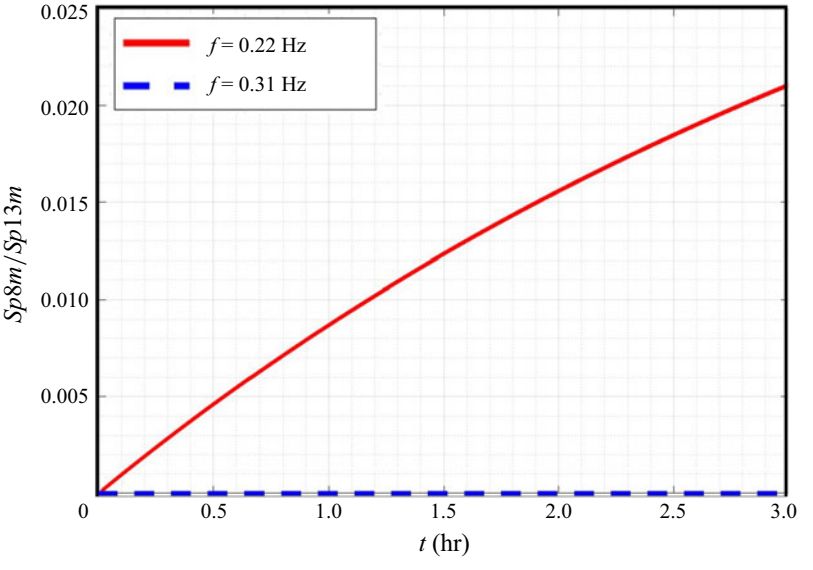

Figure 12. Seafloor pressure Fourier coefficients in 8 m water depth relative to those in 13 m water depth due to wave–wave–seafloor interactions for $f_1 = 0.10$ and $f_2 = 0.12$ Hz leading to $f_3 = 0.22$ Hz (red curve) and $f_1 = 0.15$ and $f_2 = 0.16$ Hz leading to $f_3 = 0.31$ Hz (blue curve) versus time.

likely does not contribute significantly to energy loss at low frequencies. Energy also can be lost by direct breaking of the low-frequency waves (de Bakker A. *et al.* 2014) and by nonlinear transfers from low- to higher-frequency motions (Henderson *et al.* 2006; Thomson *et al.* 2006; Bertin *et al.* 2018, and many others), whereas energy can be gained owing to nonlinear transfers among triads of waves with two swell frequencies and their low-frequency difference (Freilich & Guza 1984; Elgar & Guza 1985). In the surf zone these mechanisms oppose each other, resulting in only small changes to low-frequency spectral densities (Henderson *et al.* 2006). The observed bottom pressure spectral densities

for $f \leqslant 0.03$ Hz in 8 m depth are 200 % larger than those in 13 m depth (figure 2). Approximately 70 % of that increase could be owing to nonlinear transfers from swell as mentioned above, and from shoaling of both free and forced surface gravity waves (Elgar *et al.* 1992), with some of the rest caused by the nonlinear interactions between waves and the seafloor discussed here.

9. Discussion

The results discussed here are subject to the uncertainties arising from imprecise estimates of the Lamé constants at the test site and the dissipation coefficients (Appendix A). Further, it is expected that the predicted pressures and power densities will be lower when the incoming surface-wave field is directionally spread. This effect needs to be investigated further in follow-on work.

In view of the sensitivity of the acoustic-gravity wave field to seafloor properties, more accurate estimates for the seafloor Lamé constants and density should be derived based on samples of the seafloor characteristics at the site of interest. Similarly, more detailed representations for dissipation in the seafloor layers and in the water column at low frequencies would allow for more accurate estimation of seafloor pressures and power densities, as well as seafloor wave amplitudes. Use of a multilayered model for the seafloor should be considered for improved representation of the seafloor Lamé constants and densities. A multilayered seafloor representation also would allow for greater resolution in the dispersion relation for the underwater wave field. The approach taken here was to derive the dispersion relations using the interface conditions for the ocean-seafloor system, for an undisturbed sea surface and seafloor, with the second-order pressures imposed as forcing applied either to the sea surface (as with wave–wave interactions on the sea surface) or on the seafloor (as with surface-wave–seafloor interactions). The effect of the forcing due to the gravity term (Bondi 1947; Abdolali & Kirby 2017; Abdolali *et al.* 2019) in the compression wave–seafloor wave system should be investigated further, particularly in potential extensions of this work into the infragravity frequency range. More accurate models for the surface-wave reflection coefficient for shoreward waves will enable greater accuracy, although these may require better knowledge of the bathymetry near the site of interest.

10. Conclusions

Acoustic-gravity–Scholte waves generated by three types of nonlinear interactions involving a variable-depth elastic seafloor under a shallow compressible ocean layer were investigated. The theory applies to interactions between shoreward surface waves and the seafloor, shoreward wave fields, reflected wave fields and the seafloor, and acoustic-gravity waves and the seafloor. Surface waves were assumed to be a stationary random process. Wavenumber spectra for the forcing due to the different wave interactions were derived. Dispersion relations were derived for the acoustic-gravity–Scholte wave field, and to account for variable water depth a perturbation technique was used to obtain acoustic-gravity–Scholte wave fields up to third order. For interactions producing wavenumber–frequency combinations lying on a dispersion surface, resonant excitation of acoustic-gravity–Scholte wave groups was studied using energy balance relations that led to the forced-wave wavenumber–frequency spectra for acoustic-gravity–Scholte wave fields. Dissipation coefficients for the seafloor top layers were based on empirical observations reported in the literature. Seafloor pressure amplitudes, seafloor power densities and Scholte wave amplitudes were found. Nonlinear interactions between acoustic-gravity waves (generated by surface-wave–seafloor interactions) and the seafloor did not lead to

appreciable pressure amplitudes. In contrast, nonlinear interactions between shoreward propagating surface waves, seaward propagating reflected surface waves and the seafloor generated appreciable seafloor pressures, power spectral densities and Scholte wave amplitudes, although the sensitivity of these results to interacting frequency–wavenumber combinations needs to be examined in future work.

Propagating wave groups excited by interactions in 25 m water depth that undergo resonant amplification within the region leading up to 8 m water depth were investigated, and the second-order pressures, power densities and Scholte wave amplitudes were found to be appreciable at frequencies $f = 0.01$, 0.02, 0.03, possibly contributing to the 200 % increase in bottom pressure observed between 25 and 8 m water depths offshore of the Outer Banks of North Carolina. In addition, the nonlinear interactions may have contributed to the increase in power between 25 and 8 m depth observed at $f = 0.22$ Hz.

Seafloor power densities and seafloor pressure amplitudes available to potential resonant arrays of energy converters on the seafloor (due to the nonlinear interactions studied here) were significant over the $0.01 \leqslant f \leqslant 0.03$ Hz range. Wave–wave–seafloor interactions also led to appreciable values at $f = 0.22$ Hz. It is expected that when integrated over a seafloor area and a wider frequency range, the power values may be large enough to be of interest to applications requiring persistent power generation on the coastal seafloor. The seafloor pressure and power density results were sensitive to the seafloor mechanical properties and seafloor slope. Hence, some locations may be more attractive for seafloor power generation applications. Further, the results reported here only reflect the contribution of wave elevations in 25 m depth to the seafloor pressures in 8 m depth, and the measured pressures in 8 m depth are a cumulative result of the seafloor pressures generated by waves directly overhead and due to nonlinear interactions over the region between the two depths.

Acknowledgements. We thank T. Herbers and B. Guza for many discussions about nonlinear waves, and the CCS and FRF field crews for obtaining the observations in 13 and 8 m water depths. Funding was provided by the Office of Naval Research and the National Science Foundation. Thanks are due to H. Scott Coombe and K. Binkley for their support of this work.

Declaration of interests. The authors report no conflicts of interest.

Appendix A. Effect of the gravity term and sensitivity to parameters

A.1. *Effect of the gravity term*

A gravity contribution arises on the water surface when compressibility of the ocean layer is taken into account (Bondi 1947; Abdolali & Kirby 2017; Abdolali *et al.* 2019). A similar effect also is produced on an elastic seafloor (Abdolali *et al.* 2019). Moreover, not including this term leads to inaccuracies in the phase velocity of the surface disturbance (Abdolali *et al.* 2019), which propagates into predictions of tsunami arrival times. Here, the focus is on predicting the pressures generated at the seafloor due to surface-wave–seafloor and surface-wave–surface-wave–seafloor interactions. In addition, for the frequencies and wavenumbers of interest, the non-dimensional gravity contribution is more than an order-of-magnitude smaller than the non-dimensional quantities $\overline{k}$, $\overline{\gamma}$, and $\overline{\gamma_p}$, $\overline{\gamma_s}$.

Specifically, using the non-dimensional quantity $\overline{\Lambda_i} = gh/(2c_i^2)$ where $i = 1,\ p,\ s$, respectively (Abdolali *et al.* 2019), together with the normalizing parameters H for length and $\sqrt{H/g}$ for time and using $\bar{\cdot}$ to represent non-dimensional quantities, the non-dimensional $\overline{\gamma} = \sqrt{H^2(k^2+\alpha^2)} = \sqrt{(H/g)}\omega/(c_1/\sqrt{gH})$ equals $H(\omega/c_1)$, leading to the ratio $\overline{\Lambda_1}/\overline{\gamma} = g/(2c_1\omega)$. Similarly, the ratio of Λ_1 to a non-dimensional $\overline{k} = Hk$ equals $g/(2c_1^2 k)$. For the approximate horizontal wavenumber range $k \in (3.2 \times 10^{-5}, 3.12 \times 10^{-3})$ of interest here (approximate frequency range from 0.01 to 0.50 Hz). The ratios

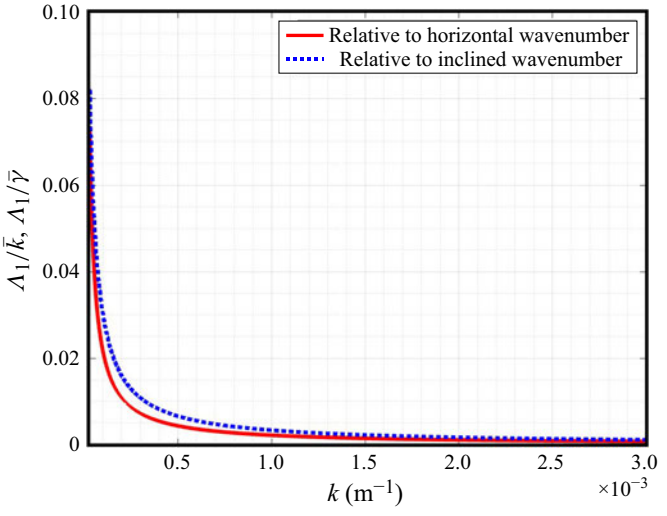

Figure 13. The ratios of the non-dimensional gravity parameter (Abdolali *et al.* 2019) to the non-dimensional horizontal wavenumber $\bar{k}$ (red curve) and to the non-dimensional inclined wavenumber $\overline{\gamma}$ (blue curve) versus wavenumber.

$\overline{\Lambda_1}/\bar{k}$ and $\overline{\Lambda_1}/\overline{\gamma}$ decrease rapidly with wavenumber (figure 13). For the 8 to 13 m water depths under consideration, and since $c_p > c_s > c_1$ here, $\Lambda_p < \Lambda_s < \Lambda_1$. The effect of the gravity term increases for $k < 3.2 \times 10^{-5}$ (or $f < 0.01$ Hz) (figure 13), qualitatively consistent with previous results (Abdolali *et al.* 2019).

A.2. *Sensitivity to parameters*

The mechanical properties (particularly, elastic moduli) of the seafloor play an important role due to their influence on the dispersion relations for the acoustic-gravity–Scholte wave system (see (5.22) and (5.27)). An uncertainty in the dispersion relations results in an uncertainty in the $(\omega, \boldsymbol{k})$ combinations at which resonances are predicted, impacting the wavenumbers at which the predicted pressure and power densities for a given frequency (or conversely, the frequency for a given wavenumber) will occur. Uncertainties in the seafloor elastic moduli also propagate into the acoustic-wave pressure spectra (6.10) and (6.12).

Additionally, the frictional losses incurred by the compression waves in the water as they travel over the bottom and through the seawater medium directly affect the seafloor power densities available for potential conversion. The seafloor mechanical properties and frictional loss coefficients over the seafloor and in seawater usually are not known precisely, and thus it is important to quantify the sensitivity of the pressure and power density estimates to uncertainties in these parameters. Tidal modulations of water depth also impact the dispersion relations, particularly in shallow water. The effects of these uncertainties on the dispersion relation and the acoustic-gravity wave pressure spectra are examined below.

A.2.1. *Sensitivity to uncertainties in the Lamé constants*

Using (5.26) for the first-order term in the perturbation expansion for mode one and dropping the subscripts and superscripts on ω, k and α for simplicity, for unidirectional

propagation,

$$D_1(\omega, k, \lambda, \lambda', \mu') = -\alpha \cos \alpha H \left(A(\lambda', \mu')D(\mu') - B(\mu')C(\mu')\right) + \rho\omega^2 \left(-\alpha' D(\mu') + ikC(\mu')\right) = 0, \tag{A1}$$

where

$$A(\lambda', \mu') = \lambda'(k^2 - \alpha^2) - 2mu'\alpha'^2; \quad B(\mu') = 2i\mu' k\beta',$$
$$C(\mu') = 2ik\mu'\alpha'; \quad D(\mu') = \mu'(k^2 + \beta'^2). \tag{A2}$$

On a dispersion surface,

$$\mathrm{d}D_1 = \frac{\partial D_1}{\partial \omega}\delta\omega + \frac{\partial D_1}{\partial \lambda'}\delta\lambda' + \frac{\partial D_1}{\partial \mu'}\delta\mu' = 0, \tag{A3}$$

where the individual partial derivatives are

$$\frac{\partial D_1}{\partial \omega}\delta\omega = 2\rho\omega \sin \alpha H \left(-\alpha' D(\mu') - ikC(\mu')\right)\delta\omega,$$
$$\frac{\partial D_1}{\partial \lambda'}\delta\lambda' = -\alpha \cos \alpha H \left(\frac{\partial A}{\partial \lambda'}D(\mu')\right)\delta\lambda',$$
$$\frac{\partial D_1}{\partial \mu'} = -\alpha \cos \alpha H \left(\frac{\partial A}{\partial \mu'}D(\mu') + A(\lambda', \mu')\frac{\partial D}{\partial \mu'} - \frac{\partial B}{\partial \mu'}C(\mu') - B(\mu')\frac{\partial C}{\partial \mu'}\right)\delta\mu', \tag{A4}$$

with the functions A, B, C and D as defined in (A2). The dispersion relation has to be satisfied on the surface $D_1(\omega, k, \lambda, \lambda', \mu') = 0$, $\mathrm{d}D_1 = 0$, so that, after appropriate substitutions and some algebra, the change $\delta\omega$ in the frequency can be related to the uncertainties $\delta\lambda'$ and $\delta\mu'$ as

$$\delta\omega = \frac{\alpha}{2\rho\omega \tanh \alpha H}\left[\frac{\left(k^2 - \alpha'^2\right)\left(k^2 + \beta'^2\right)}{-\alpha'\left(k^2 + \beta'^2\right) - 2k^2\alpha'}\delta\lambda' - \frac{2\alpha'^2\left(k^2 + \beta'^2\right) + 4k^2\beta'\alpha'}{-\alpha'\left(k^2 + \beta'^2\right) - 2k^2\alpha'}\delta\mu'\right]. \tag{A5}$$

For small depths and small values of α,

$$\lim_{\alpha H \to 0} \frac{\alpha}{\tanh \alpha H} = \frac{1}{H}. \tag{A6}$$

Dividing both sides of equation (A5) by ω for small depths, an approximate relationship can be formed,

$$\frac{\delta\omega}{\omega} = \frac{1}{2\rho\omega^2 H}\left[\frac{\left(k^2 - \alpha'^2\right)\left(k^2 + \beta'^2\right)}{-\alpha'\left(k^2 + \beta'^2\right) - 2k^2\alpha'}\delta\lambda' - \frac{2\alpha'^2\left(k^2 + \beta'^2\right) + 4k^2\beta'\alpha'}{-\alpha'\left(k^2 + \beta'^2\right) - 2k^2\alpha'}\delta\mu'\right]. \tag{A7}$$

Using the relation $\rho\omega^2 = \lambda\gamma^2$ equation (A7) can be expressed as

$$\frac{\delta\omega}{\omega} = \frac{1}{2\gamma^2 H}\left[\frac{\left(k^2 - \alpha'^2\right)\left(k^2 + \beta'^2\right)}{-\alpha'\left(k^2 + \beta'^2\right) - 2k^2\alpha'}\frac{\delta\lambda'}{\lambda} - \frac{2\alpha'^2\left(k^2 + \beta'^2\right) + 4k^2\beta'\alpha'}{-\alpha'\left(k^2 + \beta'^2\right) - 2k^2\alpha'}\frac{\delta\mu'}{\lambda}\right]. \tag{A8}$$

In (A8), with γ, k and α all being $\leqslant O(10^{-3})$ and $\lambda \sim O(10^9)$ for seawater the terms multiplying $\delta\lambda'/\lambda$ and $\delta\mu'/\lambda$ are both $O(10^3)$. Therefore, as long as $\delta\lambda'/\lambda$ and $\delta\mu'/\lambda$ are $O(10^{-3})$, the terms in the bracket are $O(10^0)$. In this case, when the depth H is $O(10^1)$, $\delta\omega/\omega$ would be $O(10^{-1})$ and the uncertainty on the frequency predicted (for a given wavenumber) by the dispersion relations would be of the order of 10 %.

For seafloor phase velocities $c_p^2 = (\lambda' + 2\mu')/\rho')$ and $c_s^2 = \mu'/\rho'$, with λ' and μ' determined from the c_p and c_s, the $\delta\omega/\omega \sim O(10^{-1})$ target above implies that $\delta c_p/c_p$ and $\delta c_s/c_s \sim O(10^{-3})$. Alternatively, it may be more preferable to use the λ' and μ' values based on laboratory analysis of samples of the seafloor surface layers and laboratory measurement of the acoustic velocities of the different constituents.

The uncertainty in the forced-wave pressure spectra (6.11) (6.15) can be estimated when the surface-wave–seafloor interaction reaches steady state after a time period much longer than the surface-wave periods, with $\mathrm{d}S_A/\mathrm{d}t = 0$, and when t is long enough for dissipation effects to dominate over spreading effects,

$$S_A(\boldsymbol{k}, t) \to \frac{\pi D_f^2}{2\omega_1^2 c_t} S_E(\omega, \boldsymbol{k}). \tag{A9}$$

The uncertainty in S_A due to uncertainties in λ' and μ' can be expressed as

$$\delta S_A = \frac{\partial S_A}{\partial \lambda'}\delta\lambda' + \frac{\partial S_A}{\partial \mu'}\delta\mu'. \tag{A10}$$

Here λ' and μ' appear explicitly in the coefficient D_f, and hence

$$\begin{aligned}\frac{\partial S_A}{\partial \lambda'} &= \frac{\pi D_f}{\omega^2 c_t}\frac{\partial D_f}{\partial \lambda'} S_E(\omega, \boldsymbol{k}),\\ \frac{\partial S_A}{\partial \mu'} &= \frac{\pi D_f}{\omega^2 c_t}\frac{\partial D_f}{\partial \mu'} S_E(\omega, \boldsymbol{k}).\end{aligned} \tag{A11}$$

At a long-enough t, dividing (A10) by S_A,

$$\frac{\delta S_A}{S_A} = \frac{2}{D_f}\left(\frac{\partial D_f}{\partial \lambda'}\delta\lambda' + \frac{\partial S_A}{\partial \mu'}\delta\mu'\right). \tag{A12}$$

Now, letting $D_d = f_0 + Af_2 + Bf_3 = 1/D_f$,

$$\begin{aligned}\frac{\partial D_f}{\partial \lambda'} &= -\frac{1}{D_d^2}\frac{\partial A}{\partial \lambda'} f_2,\\ \frac{\partial D_f}{\partial \mu'} &= -\frac{1}{D_d^2}\left(\frac{\partial A}{\partial \mu'} f_2 + \frac{\partial B}{\partial \mu'} f_3\right).\end{aligned} \tag{A13}$$

Substitutions for A, B, C and D from (6.7) and (6.8), it is found that

$$\frac{\delta S_A}{S_A} = 2D_f\left[-\left(k^2 - \alpha'^2\right) f_2 \delta\lambda' + (\alpha'^2 f_2 - ik\beta' f_3)\delta\mu'\right]. \tag{A14}$$

For realistic values of α, k, α' and β' (i.e. $\leqslant O(10^{-3})$ and $H \sim O(10^1)$, then $D_f \leqslant O(10^1)$ when $\delta\lambda'$ and $\delta\mu' \leqslant O(10^6)$, $\delta S_A/S_A < O(10^{-1})$, or less than 10 %, which provides another reason to restrict the uncertainty in the seafloor elastic constants to be $\delta\lambda'/\lambda$ and $\delta\mu'/\lambda$ to $O(10^3)$, as inferred in the discussion above of the sensitivity of the dispersion relations.

A.2.2. *Sensitivity to frictional dissipation parameters*

The predicted seafloor pressure also could be sensitive to uncertainties in the friction parameter c_t in (6.15) that accounts for the combined dissipation in the seafloor top layers and the water medium affecting the propagation of the compression wave. Following the argument for steady-state interactions (Appendix A.2.1), when dissipation effects begin to

dominate spreading,

$$S_A(\boldsymbol{k}, t) \rightarrow \frac{\pi D_1^2}{2\omega_1^2 c_t} S_E(\omega, \boldsymbol{k}), \tag{A15}$$

and

$$\delta S_A(\boldsymbol{k}, t) = \frac{\partial S_A}{\partial c_t}\delta c_t = \frac{\pi D_1^2}{2\omega_1^2} S_E(\omega, \boldsymbol{k}) \left(\frac{1}{c_t^2}\right) \delta c_t. \tag{A16}$$

Dividing throughout by S_A,

$$\frac{\delta S_A}{S_A} = \frac{\delta c_t}{c_t}. \tag{A17}$$

Since the pressure spectrum $S_P = (\lambda\gamma^2)^2 S_A$, and λ and γ are independent of c_t,

$$\frac{\delta S_P}{S_P} = \frac{\delta c_t}{c_t}. \tag{A18}$$

Therefore, when the interaction time is $> \sim 20$ min, a 10 % uncertainty in c_t will translate into a 10 % uncertainty in the predicted pressure spectra.

A.3. *Sensitivity to water depth*

The pressure spectrum due to surface-wave–seafloor interaction is given by (2.32) as

$$S_{P_\Delta}(\boldsymbol{k}, t) = \rho^2 g^2 \int_{\boldsymbol{k}} \left(\frac{\tanh \kappa H}{\cosh \kappa H}\right)^2 \kappa^2 S_e(\boldsymbol{\kappa}, t) S_f(\boldsymbol{k}_s) \delta(\boldsymbol{k} - \boldsymbol{\kappa} - \boldsymbol{k}_s) \mathrm{d}\boldsymbol{k}. \tag{A19}$$

For long surface waves and in shallow water, κH is small, $\kappa H \rightarrow 0$, and thus $\tanh \kappa H \rightarrow \kappa H$ and $\cosh \kappa H \rightarrow 1$, resulting in

$$S_{P_\Delta}(\boldsymbol{k}, t) = \rho^2 g^2 \int_{\boldsymbol{k}} (\kappa H)^2 \kappa^2 S_e(\boldsymbol{\kappa}, t) S_f(\boldsymbol{k}_s) \delta(\boldsymbol{k} - \boldsymbol{\kappa} - \boldsymbol{k}_s) \mathrm{d}\boldsymbol{k}. \tag{A20}$$

In this case,

$$\delta S_{P_\Delta} = \frac{\partial S_{P_\Delta}}{\partial H}\delta H, \tag{A21}$$

which leads to

$$\begin{aligned} \delta S_{P_\Delta} &= 2\rho^2 g^2 \int_{\boldsymbol{k}} (\kappa^2 H) \kappa^2 S_e(\boldsymbol{\kappa}, t) S_f(\boldsymbol{k}_s) \delta(\boldsymbol{k} - \boldsymbol{\kappa} - \boldsymbol{k}_s) \mathrm{d}\boldsymbol{k}, \\ &= 2\rho^2 g^2 \int_{\boldsymbol{k}} \frac{(\kappa H)^2}{H} \kappa^2 S_e(\boldsymbol{\kappa}, t) S_f(\boldsymbol{k}_s) \delta(\boldsymbol{k} - \boldsymbol{\kappa} - \boldsymbol{k}_s) \mathrm{d}\boldsymbol{k}, \\ \Rightarrow \frac{\delta S_{P_\Delta}}{S_{P_\Delta}} &= \frac{2\delta H}{H}. \end{aligned} \tag{A22}$$

Thus, within the small κH approximation, a 10 % uncertainty in water depth H would result in a 20 % uncertainty in the pressure spectrum. Here, the depths of the observations (figure 2) H were measured, and thus the uncertainty is less than a few per cent.

References

Abdolali, A., Kadri, U. & Kirby, J.T. 2019 Effect of water compressibility, sea-floor elasticity, and field gravitational potential on tsunami phase speed. *Sci. Rep.* **9** (1), 16874.

Abdolali, A. & Kirby, J.T. 2017 Role of compressibility on tsunami propagation. *J. Geophys. Res.: Oceans* **122**, 9780–9794.

Ardhuin, F. 2018 Large-scale forces under surface gravity waves at a wavy bottom: a mechanism for generation of primary microseisms. *Geophys. Res. Lett.* **45**, 8173–8181.

Ardhuin, F., Gualtieri, L. & Strutzmann, E. 2015 How ocean waves rock the earth: two mechanisms explain microseisms with periods 2s to 300s. *Geophys. Res. Lett.* **42**, 765–722.

Ardhuin, F. & Herbers, T.H.C. 2013 Noise generation in the solid Earth, oceans, and atmosphere, from nonlinear interacting surface gravity waves in finite depth. *J. Fluid Mech.* **716**, 316–348.

Arduin, F., Drake, T. & Herbers, T. 2002 Observations of wave-generated vortex ripples on the North Carolina continental shelf. *J. Geophys. Res.* **107**, 3143.

Auld, B.A. 1990 *Acoustic Fields and Waves in Solids*, 2nd edn, vol. I. Krieger Publishing.

de Bakker, A., Tissier, M. & Ruessink, B. 2014 Shoreline dissipation of infragravity waves. *Cont. Shelf Res.* **72**, 73–82.

Bertin, X., *et al.* 2018 Infragravity waves: from driving mechanisms to impacts. *Earth Sci. Rev.* **177**, 774–799.

Bondi, H. 1947 Waves on the surface of a compressible liquid. *Math. Proc. Camb. Phil. Soc.* **43** (1), 75–95.

Bromirski, P.D., Stephen, R.A. & Gerstoff, P. 2013 Are deep-ocean-generated surface-wave microseisms observed on land. *J. Geophys. Res.: Solid Earth* **118**, 3610–3629.

Dunnebier, F.K., Lukas, R., Nosal, E.-M., Aucan, J. & Weller, R.A. 2012 Wind, waves, and acoustic background levels at station ALOHA. *J. Geophys. Res.* **117** (C03017), 1–21.

Dziewonski, A.M. & Anderson, D.L. 1981 Preliminary reference Earth model. *Phys. Earth Planet. Inter.* **25**, 297–356.

Elgar, S. & Guza, R.T. 1985 Observations of bispectra of shoaling surface gravity waves. *J. Fluid Mech.* **161**, 425–448.

Elgar, S., Guza, R.T., Raubenheimer, B., Herbers, T.H.C. & Gallagher, E. 1997 Spectral evolution of shoaling and breaking waves on a barred beach. *J. Geophys. Res.* **1002**, 15797–15805.

Elgar, S., Herbers, T.H.C., Chandran, V. & Guza, R.T. 1995 Higher-order spectral analysis of nonlinear ocean surface gravity waves. *J. Geophys. Res.* **100**, 4977–4983.

Elgar, S., Herbers, T.H.C. & Guza, R.T. 1994 Reflection of ocean surface gravity waves from a natural beach. *J. Phys. Oceanogr.* **24**, 1503–1511.

Elgar, S., Herbers, T.H.C., Okihiro, M., Oltman-Shay, J. & Guza, R.T. 1992 Observations of infragravity waves. *J. Geophys. Res.* **97** (15), 573–577.

Eyov, E., Klar, A., Kadri, U. & Stiassnie, M. 2013 Progressive waves in a compressible-ocean with an elastic bottom. *Wave Motion* **50**, 929–939.

Freilich, M.H. & Guza, R.T. 1984 Nonlinear effects of shoaling surface gravity waves. *Phil. Trans. R. Soc. Lond. A* **311**, 1–41.

Gottwald, J.T. 1970 Acoustic atteuation in the deep ocean below 2000 Hz. *Tech. Rep.* T-70-WA-2001-U. Tracor Inc, Washington, DC.

Graff, K.F. 1991 *Wave Motion in Elastic Solids*. Dover Publications, reissue of Oxford University Press 1975 edition.

Hasselmann, K. 1962 On the nonlinear energy transfer in a gravity-wave spectrum. *J. Fluid Mech.* **12**, 481–450.

Hasselmann, K. 1963 A statistical analysis of the generation of microseisms. *Rev. Geophys.* **1** (2), 177–210.

Hasselmann, K. 1966 Feynman diagrams and interaction rules of wave-wave scattering processes. *Rev. Geophys.* **4** (1), 1–32.

Hasselmann, K. 1976 Stochastic climate models part I, theory. *Tellus* **26** (6), 473–485.

Henderson, S.M., Guza, R.T., Elgar, S., Herbers, T.H.C. & Bowen, A.J. 2006 Nonlinear generation and loss of infragravity wave energy. *J. Geophys. Res.* **111**, C12007.

Herbers, T.H.C. & Guza, R.T. 1991 Wind-wave nonlinearity observed at the seafloor. Part I: forced-wave energy. *J. Phys. Oceanogr.* **21**, 1740–1761.

Herbers, T.H.C. & Guza, R.T. 1994 Nonlinear wave interactions and high-frequency seafloor pressure. *J. Geophys. Res.* **99** (C5), 10035–10048.

Hughes, B. 1976 Estimates of underwater sound (and infrasound) produced by nonlinearly interacting ocean waves. *J. Acoust. Soc. Am.* **60** (5), 1032–1039.

Jensen, F.B., Kuperman, W.A., Porter, M.B. & Schmidt, H. 2011 *Computational Ocean Acoustics*, 2nd edn. Springer.

KADRI, U. & AKYLAS, T.R. 2016 On resonant triad interaction of acoustic-gravity waves. *J. Fluid Mech.* **788** (R1), 788R1–788R12.

KAIHATU, J. & KIRBY, J. 1992 Spectral evolution of directional finite amplitude dispersive waves in shallow water. *Proc. Intl Conf. Coast. Engng* **26**, 364–377.

KAIHATU, J. & KIRBY, J. 1995 Nonlinear transformation of waves in finite water depth. *Phys. Fluids* **7** (8), 1903–1914.

KIBBLEWHITE, A.C. 1989 Attenuation of sound in marine sediments: a review with emphasis on new low-frequency data. *J. Acoust. Soc. Am.* **86**, 716–738.

KIBBLEWHITE, A.C. & WU, C.Y. 1993 Acoustic source levels associated with the nonlinear interactions of ocean waves. *J. Acoust. Soc. Am.* **94**, 3358–3378.

KIRBY, J. 1992 Modelling shoaling directional wave spectra in shallow water. *Proc. Intl Conf. Coast. Engng* **8**, 109–122.

KOMEN, G.J. & HASSELMANN, K. 1996 The action balance equation and the statistical description of wave evolution. In *Dynamics and Modelling of Ocean Waves* (ed. G.J. KOMEN, L. CAVALERI, M. DONELAN, K. HASSELMANN, S. HASSELMANN & P.A.E.M. JANSEN), pp. 5–47. Cambridge University Press.

KORDE, U.A. 2024 Propagation of underwater wave groups in a compressible ocean coupled with an elastic seafloor. *J. Fluid Mech.* **996** (A18), 1–44.

KORDE, U.A. & MCBETH, M.S. 2022 On using nonlinear wave interactions in multi-directional seas for energy conversion on the ocean floor. *Appl. Ocean Res.* **124**, 103193.

LONGUET-HIGGINS, M.S. 1950 A theory of the origin of microseisms. *Phil. Trans. R. Soc. Lond. A Math. Phys. Sci.* **243** (857), 1–35.

MASE, H. & KIRBY, J. 1992 Hybrid frequency-domain KdV equation for random wave transformation. In *Proceedings of the Twenty-Third International Conference on Coastal Engineering, October, Venice, Italy*, pp. 474–487.

MEISBURGER, E.P., JUDGE, C. & WILLIAMS, E.J. 1989 Physiographic and geological setting of the coastal engineering research center facility. *Tech. Rep.* CERC-89-9. US Army Waterways Experiment Station.

MEZA-VALLE, C., KADRI, U. & ORTEGA, J.H. 2023 Acoustic-gravity waves generated by surface disturbances. *Eur. J. Mech. B/Fluids* **98**, 1–7.

MICHELE, S. & RENZI, E. 2020 Effects of the sound speed vertical profile on the evolution of hydroacoustic waves. *J. Fluid Mech.* **883** (A28), 1–12.

OLIVER, J. 1962 A worldwide storm of microseisms with periods of about 27 seconds. *Bull. Seismol. Soc. Am.* **52** (3), 507–512.

PHILLIPS, O.M. 1960 On the dynamics of unsteady gravity waves of finite amplitude, 1, the elementary interactions. *J. Fluid Mech.* **9**, 193–217.

RENZI, E. 2017 Hydro-acoustic frequencies of the weakly compressible mild-slope equation. *J. Fluid Mech.* **812**, 5–25.

RENZI, E. & DIAS, F. 2014 Hydroacoustic precursors of gravity waves generated by surface pressure disturbances localized in space and time. *J. Fluid Mech.* **754**, 250–262.

STIASSNIE, M. 2010 Tsunamis and acoustic-gravity waves from underwater earthquakes. *J. Engng Maths* **67**, 23–32.

THOMSON, J., ELGAR, S., RAUBENHEIMER, B., HERBERS, T.H.C. & GUZA, R.T. 2006 Tidal modulation of infragravity waves via nonlinear energy losses in the surf zone. *Geophys. Res. Lett.* **33**, L05601.

TURGUT, A. & YAMAMOTO, T. 1990 Measurements of acoustic wave velocities and attenuation in marine sediments. *J. Acoust. Soc. Am.* **87**, 2376–2383.

WANG, C., WEI, Y., CHEN, W. & HUANG, L. 2024 Hydroelastic modelling of a deformable wave energy converter including power take-off. *Mar. Struct.* **98**, 103678.

WEBB, S.C. & COX, C.S. 1986 Observations and modeling of seafloor microseisms. *J. Geophys. Res.* **91** (7), 7343–7358.

WEBB, S.C. & CRAWFORD, W.C. 1999 Long-period seafloor seismology and deformation under ocean waves. *Bull. Seismol. Soc. Am.* **89** (6), 1532–1542.

WHITHAM, G.B. 1973 *Linear and Nonlinear Waves*. John Wiley & Sons, NY, a Wiley-Interscience Publication.

WILLIAMS, B. & KADRI, U. 2023 On the propagation of acoustic-gravity waves due to a slender rupture in an elastic seabed. *J. Fluid Mech.* **956** (A6), A6–1–44.